INTERNATIONAL JOURNAL FOR NUMERICAL METHODS IN FLUIDS
*Int. J. Numer. Meth. Fluids* 2014; **76**:282–311
Published online 12 July 2014 in Wiley Online Library (wileyonlinelibrary.com). DOI: 10.1002/fld.3934

RESEARCH PAPER PRESENTED AT THE 8TH SYMPOSIUM ON NUMERICAL ANALYSIS OF FLUID FLOW AND HEAT TRANSFER 2013

# A compressible single-temperature conservative two-phase model with phase transitions

G. La Spina[1,2,*,†], M. de' Michieli Vitturi[1] and E. Romenski[3]

[1]*Istituto Nazionale di Geofisica e Vulcanologia, Sezione di Pisa, Italy*
[2]*Dipartimento di Matematica L.Tonelli, University of Pisa, Pisa, Italy*
[3]*Sobolev Institute of Mathematics, Russian Academy of Sciences, Moscow, Russia*

SUMMARY

A model for multidimensional compressible two-phase flow with pressure and velocity relaxations based on the theory of thermodynamically compatible system is extended to study liquid–gas flows with cavitation. The model assumes for each phase its own pressure and velocity, while a common temperature is considered. The governing equations form a hyperbolic system in conservative form and are derived through the theory of a thermodynamically compatible system. The phase pressure-equalizing process and the interfacial friction are taken into account in the balance laws for the volume fractions of one phase and for the relative velocity by adding two relaxation source terms, while the phase transition is introduced into the model considering in the balance equation for the mass of one phase the relaxation of the Gibbs free energies of the two phases. A modification of the central finite-volume Kurganov–Noelle–Petrova method is adopted in this work to solve the homogeneous hyperbolic part, while the relaxation source terms are treated implicitly. In order to investigate the effect of the mass transfer in the solution, a 1D cavitation tube problem is presented. In addition, two 2D numerical simulations regarding cavitation problem are also studied: a cavitating Richtmyer–Meshkov instability and a laser-induced cavitation problem. Copyright © 2014 John Wiley & Sons, Ltd.

Received 1 February 2014; Revised 22 April 2014; Accepted 9 June 2014

KEY WORDS: compressible flow; finite volume; hyperbolic; partial differential equations; two-phase flows; phase change

## 1. INTRODUCTION

Multiphase flow modeling is one of the most challenging research areas in computational and applied mathematics, and intensive efforts have been carried out in the recent decades in the development of advanced models and numerical methods. Common formulations of mathematical models of multiphase flows are originated in [1, 2] and are based on the averaging theory. The governing equations of such models consist of the balance equations for density, momentum, and energy of each phase, and phase interaction is taken into account by additional algebraic and differential source terms. The model proposed by Baer and Nunziato [2] and studied in [3] stimulated further modifications of the governing equations and the development of new approaches in the modeling of two-phase flows (e.g., [4–6]). In these papers and references therein, the mathematical properties of differential equations of two-phase flow models were studied, and a variety of test

*Correspondence to: G. La Spina, Istituto Nazionale di Geofisica e Vulcanologia, Sezione di Pisa, via della Faggiola, 32, Pisa, 56126, Italy.
†E-mail: giuseppe.laspina@pi.ingv.it

problems have been solved numerically. It is proven that the differential equations of the model are hyperbolic, which guarantees the solvability of certain classes of initial-boundary-value problems. One disadvantage of the Baer–Nunziato-type models is that not all equations can be written in a conservative (divergent) form. Note that the divergent form of equations is very attractive because it allows application of known mathematical tools and accurate numerical methods to study problems of practical interest.

Another phenomenological approach, based on the theory of thermodynamically compatible system of conservation laws was proposed in [7, 8] to formulate the governing equations of multiphase compressible flow. In this method, the mixture is supposed as a continuum in which a multiphase character of a flow is taken into account by introducing new phenomenological variables beyond the classical density, momentum, and energy. The resulting governing equations form a hyperbolic system of equations in conservative form, and these equations can be rewritten as a set of subsystems of conservation laws for each phase coupled by the interface exchange terms. In general, the two-phase-flow thermodynamically compatible equations differ from the Baer–Nunziato-type equations, but for the simplest case of 1D isentropic flow, they coincide [7].

Multiphase flow problems are very challenging even in the case of two-phase flow. That is why many papers are devoted to the development of simplified models that are designed to introduce additional constraints [9, 10]. These constraints usually represent an assumption that the rate of unsteady-state relaxation to the equilibrium state is very high as compared with the characteristic time of the process under consideration. As a rule, these constraints consist in the requirement that the pressures, velocities, or temperatures must be equal in the two phases. In recent years, two-phase models with gas–liquid transition have been developed in [11], where phase change is introduced with the use of discontinuities derived from the conservation laws. This approach requires a detailed knowledge of properties of discontinuous solution, and its numerical realization is quite complicated. Actually, the phase transition in the two-phase model can also be accounted as an irreversible process with a high rate of relaxation. In [12], a simplified two-phase model is proposed in which an equality of phase Gibbs potentials is proposed in addition to the phase velocities, pressures, and temperatures equalities. In this paper, the kinetic model of phase transition with a finite rate is proposed by adding a source term to the phase mass balance equations with phase Gibbs potential relaxation to the common value. A similar approach, for example, is used in [13] for the description of continuous phase transition in polytetrafluoroethylene.

In the present paper, phase transition is introduced in the thermodynamically compatible system of conservation laws proposed in [14, 15] for a two-phase flow with single temperature, but different pressures and velocities. Although the temperature-equalizing time is larger than the pressure and velocity relaxation times, as noted in [16], it is possible to consider a single-temperature model as an approximate model of flow if the difference of phase temperatures is not too big. Mathematical properties of the governing equations are studied, and three test problems are solved numerically. The effect of the finite rate of pressure relaxation on the pressure wave in two-phase flow is investigated, and it is shown that the solutions are significantly different for different rates. A 1D cavitation problem, as formulated in [12], is considered here with liquid–vapor evaporation. The evaporation is modeled by the nonlinear kinetics in the phase mass balance equations. It is shown that the flow character strongly depends on the nonlinearity of the kinetic coefficient as a function of temperature and pressure. We present also two multidimensional numerical tests regarding the cavitation problem: a cavitating Richtmyer–Meshkov instability simulation [17, 18] and a laser-induced cavitation problem [19].

For solving the proposed governing equations, a finite-volume numerical scheme based on the MUSCL-Hancock method with linear reconstruction [20] is adopted. The conservative form of the equations allows the use of central methods to compute the fluxes [21, 22], and in this paper, the modification of the Kurganov, Noelle, and Petrova numerical fluxes in conjunction with a second-order reconstruction presented in [15] is adopted.

This paper is organized as follows. In Section 2, we present the governing equations, and we derive an entropy balance for the system. In Section 3, the equations of state used as closure constitutive relations are described. Section 4 is devoted to the characteristic analysis of the system of equation, and more details on the evaluation of the eigenvalues are given in Appendix A.



DOI: 10.1002/fld

Section 5 describes first the modified central finite-volume scheme adopted and the details of the integration of the source terms, and finally, the numerical results are presented for three test cases.

## 2. CONSERVATIVE EQUATIONS FOR TWO-PHASE COMPRESSIBLE MODEL

### *2.1. Single-temperature governing equations*

In this section, we present the extension to liquid–gas flows with cavitation of the two-phase flow model with two pressures, two velocities, and a single temperature, which has been proposed in [14] and studied in [15]. These equations are derived using the principles of extended thermodynamics [23–26], and the resulting system of partial differential equations can be written in conservative form and transformed into a symmetric hyperbolic system in a similar way to those described in [8, 14]. Note that symmetric hyperbolic systems form a special class of hyperbolic systems in the sense of Friedrichs [27], for which the initial value problem is well posed, and a deep mathematical theory is developed (e.g., [28] and references therein). Here, we extend the model considering also phase transition, and the new entropy balance is derived in the next subsection.

In the two-phase model, each phase can be characterized by its own parameters of state. The phase volume fractions in the mixture are denoted with $\alpha_1$ and $\alpha_2$, and they satisfy the saturation constraint $\alpha_1 + \alpha_2 = 1$. Phase mass densities are $\rho_1$ and $\rho_2$, while the velocities are $\vec{u}_1$ and $\vec{u}_2$.

We introduce also the notation $s_i$ for the phase-specific entropies and $e_i$ for the specific internal energy, and we assume that the equations of state for each phase $e_i$ are known function of the density $\rho_i$ and entropy $s_i$:

$$e_i = e_i(\rho_i, s_i). \tag{1}$$

The phase pressures $p_i$ and the temperatures $T_i$ are computed from the equations of state as follows:

$$p_i = \rho_i^2 \frac{\partial e_i}{\partial \rho_i} \qquad \text{and} \qquad T_i = \frac{\partial e_i}{\partial s_i}. \tag{2}$$

Finally, the following mixture parameters of state, connected with the individual phase parameters, are introduced:

$$\begin{gathered} T = T_1 = T_2, \qquad \rho = \alpha_1\rho_1 + \alpha_2\rho_2, \qquad c = c_1 = \frac{\alpha_1\rho_1}{\rho}, \\ \vec{u} = c_1\vec{u}_1 + c_2\vec{u}_2, \qquad \vec{w} = \vec{u}_1 - \vec{u}_2, \qquad e = c_1e_1 + c_2e_2, \text{ and} \\ E = e + c(1-c)\frac{|\vec{w}|^2}{2}, \end{gathered} \tag{3}$$

where $T$ is the common temperature, $\rho$ is the mixture density, $c$ is the mass fraction of the first phase, $\vec{u}$ is the mixture velocity, $\vec{w}$ is the relative velocity, $e$ is the specific internal energy of the mixture, $c_2$ is the mass fraction of the second phase, and $E$ is the total specific energy of the mixture.

Using this notation, we can write the mixture mass conservation law:

$$\frac{\partial}{\partial t}(\rho) + \nabla \cdot \left(\rho\vec{u}\right) = 0. \tag{4}$$

The balance law for the volume fraction of the first phase is

$$\frac{\partial}{\partial t}(\rho\alpha_1) + \nabla \cdot \left(\rho\alpha_1\vec{u}\right) = -\phi, \tag{5}$$



DOI: 10.1002/fld

where $\phi$ is the pressure relaxation defined as a function of the pressures difference and a relaxation rate $\tau^{(p)}$ by

$$\phi = \frac{1}{\tau^{(p)}}(p_2 - p_1). \tag{6}$$

This term represents the phase pressure equalizing through the process of pressure wave propagation in dispersed phase and its interaction with the interface boundaries.

The mass conservation law for the first phase is

$$\frac{\partial}{\partial t}(\rho_1\alpha_1) + \nabla\cdot\left(\rho_1\alpha_1\vec{u}_1\right) = -\rho\theta, \tag{7}$$

where $\theta$ is defined as

$$\theta = \frac{1}{\tau^{(c)}}\left(\mu_1 - \mu_2 + (1-2c)\frac{|\vec{w}|^2}{2}\right). \tag{8}$$

In the previous equation, $\tau^{(c)}$ is a phase exchange relaxation rate, $\vec{w}$ is the relative velocity, and $\mu_1$ and $\mu_2$ are the phase chemical potentials (or Gibbs free energies):

$$\mu_1 = e_1 + \frac{p_1}{\rho_1} - s_1T, \qquad \mu_2 = e_2 + \frac{p_2}{\rho_2} - s_2T. \tag{9}$$

The mixture momentum equation is

$$\frac{\partial}{\partial t}\left(\rho\vec{u}\right) + \nabla\cdot\left[\vec{u}_1\otimes(\rho_1\alpha_1\vec{u}_1) + \vec{u}_2\otimes(\rho_2\alpha_2\vec{u}_2) + (\alpha_1p_1 + \alpha_2p_2)\mathbf{I}\right] = 0, \tag{10}$$

where $\mathbf{I}$ is the 3D identity matrix and $\otimes$ is the tensor product.

The relative velocity equation in conservative form is

$$\frac{\partial}{\partial t}\left(\vec{w}\right) + \nabla\cdot\left[\frac{\vec{u}_1\otimes\vec{u}_1}{2} - \frac{\vec{u}_2\otimes\vec{u}_2}{2} + \left(e_1 + \frac{p_1}{\rho_1} - e_2 - \frac{p_2}{\rho_2} - (s_1 - s_2)T\right)\mathbf{I}\right] = -\frac{1}{\rho}\vec{\lambda}_0 - \vec{u}\times\vec{\omega}, \tag{11}$$

where the interfacial friction $\vec{\lambda}_0$ is defined as a function of the interfacial friction coefficient $\zeta$, the mass fraction $c$ and the relative velocity $\vec{w}$:

$$\vec{\lambda}_0 = \zeta c(1-c)\vec{w}. \tag{12}$$

In the case of dispersed particle flow, the velocity relaxation represents the Stokes drag force in the phase momentum equations.

As was carried out in [8], to save a conservation law form of the system, in equation (11), it is introduced as an artificial vector $\vec{\omega}$ satisfying the steady-state equation

$$\nabla\times\vec{w} = \vec{\omega}. \tag{13}$$

Furthermore, this variable can be treated as a source term in the equation for the relative velocity [14].

The conservation energy law is written as

$$\begin{aligned}\frac{\partial}{\partial t}\left[\rho\left(E + \frac{|\vec{u}|^2}{2}\right)\right] + \nabla\cdot\Bigg[&\alpha_1\rho_1\vec{u}_1\left(e_1 + \frac{|\vec{u}_1|^2}{2} + \frac{p_1}{\rho_1}\right) + \alpha_2\rho_2\vec{u}_2\left(e_2 + \frac{|\vec{u}_2|^2}{2} + \frac{p_2}{\rho_2}\right)\\ &-\rho c(1-c)\vec{w}(s_1 - s_2)T\Bigg] = 0.\end{aligned} \tag{14}$$



DOI: 10.1002/fld

To summarize, introducing the vector of conservative variables $\mathbf{q}$, defined as

$$\mathbf{q} = \begin{pmatrix} \alpha_1\rho_1 + (1-\alpha_1)\rho_2 \\ \alpha_1(\alpha_1\rho_1 + (1-\alpha_1)\rho_2) \\ \alpha_1\rho_1 \\ \alpha_1\rho_1\vec{u}_1 + (1-\alpha_1)\rho_2\vec{u}_2 \\ \vec{w} \\ \rho\left(E + \frac{|\vec{u}|^2}{2}\right) \end{pmatrix}, \tag{15}$$

the system of governing partial differential equations can be written in the following more compact form:

$$\frac{\partial \mathbf{q}}{\partial t} + \nabla \cdot \mathbf{F}(\mathbf{q}) = \mathbf{\Omega}(\mathbf{q}), \tag{16}$$

where $\mathbf{F}(\mathbf{q})$ are the conservative fluxes

$$\mathbf{F}(\mathbf{q}) = \begin{pmatrix} \rho\vec{u} \\ \rho\alpha_1\vec{u} \\ \rho_1\alpha_1\vec{u_1} \\ \vec{u}_1 \otimes (\rho_1\alpha_1\vec{u}_1) + \vec{u}_2 \otimes (\rho_2\alpha_2\vec{u}_2) + (\alpha_1 p_1 + \alpha_2 p_2)\mathbf{I} \\ \dfrac{\vec{u}_1 \otimes \vec{u}_1}{2} - \dfrac{\vec{u}_2 \otimes \vec{u}_2}{2} + \left(e_1 + \dfrac{p_1}{\rho_1} - e_2 - \dfrac{p_2}{\rho_2} - (s_1 - s_2)T\right)\mathbf{I} \\ \displaystyle\sum_{i=1}^{2}\left[\alpha_i\rho_i\vec{u}_i\left(e_i + \frac{|\vec{u}_i|^2}{2} + \frac{p_i}{\rho_i}\right)\right] - \rho c(1-c)\vec{w}(s_1 - s_2)T \end{pmatrix}, \tag{17}$$

and $\mathbf{\Omega}(\mathbf{q})$ are the relaxation terms

$$\mathbf{\Omega}(\mathbf{q}) = \begin{pmatrix} 0 \\ -\dfrac{1}{\tau^{(p)}}(p_2 - p_1) \\ -\dfrac{1}{\tau^{(c)}}\rho\left(\mu_1 - \mu_2 + (1-2c)\dfrac{|\vec{w}|^2}{2}\right) \\ 0 \\ -\zeta\left[\dfrac{c(1-c)}{\rho}\vec{w}\right] - \vec{u} \times \vec{\omega} \\ 0 \end{pmatrix}. \tag{18}$$

Equations (1–3), (9), and (13) represent the closure of the partial differential equation system (16–18).

Finally, we observe that, after some cumbersome transformation, it is possible to derive for each phase a momentum balance equation. For the sake of simplicity, we present here the equations for the 1D model:

$$\begin{aligned} \frac{\partial \alpha_1\rho_1 u_1}{\partial t} + \frac{\partial\left(\alpha_1\rho_1 u_1^2 + \alpha_1 p_1\right)}{\partial x} = &\left[\frac{(\alpha_2\rho_2 p_1 + \alpha_1\rho_1 p_2)}{\rho}\right]\frac{\partial}{\partial x}\alpha_1 - \frac{\alpha_1\rho_1\alpha_2\rho_2}{\rho}(s_2 - s_1)\frac{\partial}{\partial x}T \\ &- \rho\theta u_1 + \alpha_1\rho_1\theta(u_1 - u_2) - \frac{\alpha_1\rho_1\alpha_2\rho_2}{\rho^2}\lambda_0. \end{aligned} \tag{19}$$



DOI: 10.1002/fld

$$\frac{\partial \alpha_2\rho_2 u_2}{\partial t} + \frac{\partial\left(\alpha_2\rho_2 u_2^2 + \alpha_2 p_2\right)}{\partial x} = \left[\frac{(\alpha_2\rho_2 p_1 + \alpha_1\rho_1 p_2)}{\rho}\right]\frac{\partial}{\partial x}\alpha_2 - \\ + \frac{\alpha_1\rho_1\alpha_2\rho_2}{\rho}(s_2 - s_1)\frac{\partial}{\partial x}T + \rho\theta u_2 \\ + \alpha_2\rho_2\theta(u_1 - u_2) + \frac{\alpha_1\rho_1\alpha_2\rho_2}{\rho^2}\lambda_0. \tag{20}$$

We observe that, with respect to other models based on the approach of Baer and Nunziato [2], the definition of interfacial pressure is different. As discussed in [7], while in the Baer–Nunziato-type models, we have $p_I = \alpha_1 p_1 + \alpha_2 p_2$, here, the interfacial pressure in the momentum balance equations for the two phases is expressed as

$$\hat{p}_I = \frac{\alpha_2\rho_2 p_1 + \alpha_1\rho_1 p_2}{\rho}. \tag{21}$$

An analogous dual relation was also proposed in [29] for studying the Richtmyer–Meshkov instability. In [30], the definition of the interface pressure was defined in terms of impedances of each phase. But the same duality was present.

### 2.2. *Entropy balance*

We show here that from the system of equations (4–14), it is possible to write an equation for the balance of the total mixture entropy $S$, defined as

$$S = c_1 s_1 + c_2 s_2. \tag{22}$$

From now on, for simplicity, we only consider the monodimensional case, and in this way, the steady-state equation (13) and the term $\vec{u} \times \vec{\omega}$ in the relative velocity equation can be neglected, obtaining the following system:

$$\frac{\partial}{\partial t}(\rho) + \frac{\partial}{\partial x}(\rho u) = 0, \tag{23}$$

$$\frac{\partial}{\partial t}(\rho\alpha_1) + \frac{\partial}{\partial x}(\rho\alpha_1 u) = -\phi, \tag{24}$$

$$\frac{\partial}{\partial t}(\rho_1\alpha_1) + \frac{\partial}{\partial x}(\rho_1\alpha_1 u_1) = -\rho\theta, \tag{25}$$

$$\frac{\partial}{\partial t}(\rho u) + \frac{\partial}{\partial x}\left[\rho_1\alpha_1(u_1)^2 + \rho_2\alpha_2(u_2)^2 + \alpha_1 p_1 + \alpha_2 p_2\right] = 0, \tag{26}$$

$$\frac{\partial}{\partial t}(w) + \frac{\partial}{\partial x}\left[\frac{(u_1)^2}{2} - \frac{(u_2)^2}{2} + e_1 + \frac{p_1}{\rho_1} - e_2 - \frac{p_2}{\rho_2} - (s_1 - s_2)T\right] = -\frac{1}{\rho}\lambda_0, \tag{27}$$



DOI: 10.1002/fld

$$\frac{\partial}{\partial t}\left[\rho\left(E+\frac{u^2}{2}\right)\right]+\frac{\partial}{\partial x}\left[\alpha_1\rho_1u_1\left(e_1+\frac{(u_1)^2}{2}+\frac{p_1}{\rho_1}\right)+\alpha_2\rho_2u_2\left(e_2+\frac{(u_2)^2}{2}+\frac{p_2}{\rho_2}\right)\right.$$
$$\left.-\rho c(1-c)w(s_1-s_2)T\right]=0. \tag{28}$$

To derive the entropy balance equation, first we have to write an equivalent nonconservative form of equations (23)–(28).

Using the notation for the total energy of the mixture $E$ reported in equation (3), it is possible to write an equivalent nonconservative form of equations (23)–(28) for the variables $(\alpha_1, c, \rho, u, w, E)$:

$$\begin{aligned}
&\frac{d\alpha_1}{dt}=-\frac{\phi}{\rho},\\
&\rho\frac{dc}{dt}+\frac{\partial}{\partial x}(\rho c(1-c)w)=-\rho\theta,\\
&\frac{d\rho}{dt}+\rho\frac{\partial u}{\partial x}=0,\\
&\rho\frac{du}{dt}+\frac{\partial p}{\partial x}+\frac{\partial}{\partial x}(\rho c(1-c)w^2)=0,\\
&\frac{dw}{dt}+w\frac{\partial u}{\partial x}+\frac{\partial}{\partial x}\left((1-2c)\frac{w^2}{2}+\mu_1-\mu_2\right)=-\frac{1}{\rho}\lambda_0,\\
&\rho\frac{dE}{dt}+p\frac{\partial u}{\partial x}+\rho c(1-c)w^2\frac{\partial u}{\partial x}\\
&\qquad+\frac{\partial}{\partial x}\left(\rho\left(\mu_1-\mu_2+(1-2c)\frac{w^2}{2}\right)(c(1-c)w)\right)=0,
\end{aligned} \tag{29}$$

where we used the notation $d/dt$ for the material derivative

$$\frac{d}{dt}=\frac{\partial}{\partial t}+u\frac{\partial}{\partial x}. \tag{30}$$

Now, using the formula

$$dE=\frac{\partial E}{\partial\alpha_1}d\alpha_1+\frac{\partial E}{\partial\rho}d\rho+\frac{\partial E}{\partial c}dc+\frac{\partial E}{\partial w}dw+\frac{\partial E}{\partial S}dS,$$

we find the material derivative of the total mixture entropy

$$\frac{dS}{dt}=\frac{1}{E_S}\left(\frac{dE}{dt}-E_{\alpha_1}\frac{d\alpha_1}{dt}-E_\rho\frac{d\rho}{dt}-E_c\frac{dc}{dt}-E_w\frac{dw}{dt}\right). \tag{31}$$

The partial derivatives of $E$, appearing in the previous equation, can be easily evaluated from the definition of $E$ reported in equation (3), rewriting first the specific internal energy of the mixture $e$ in terms of the mixture parameters $(\alpha_1, \rho, c, S)$:



DOI: 10.1002/fld

$$
\begin{aligned}
E_w &= c(1-c)w,\\
E_c &= \frac{\partial}{\partial c}e(\alpha_1,\rho,c,S) + (1-2c)\frac{w^2}{2} = \mu_1 - \mu_2 + (1-2c)\frac{w^2}{2},\\
E_\alpha &= \frac{p_1 - p_2}{\rho},\\
E_\rho &= \frac{1}{\rho^2}(\alpha_1 p_1 + \alpha_2 p_2),\\
E_S &= T.
\end{aligned}
$$

Using (29) and the previous expressions, we can rewrite (31) as

$$
\begin{aligned}
\frac{dS}{dT} = \frac{1}{T}\Bigg[&-\frac{p}{\rho}\frac{\partial u}{\partial x} - wE_w\frac{\partial u}{\partial x} - \frac{1}{\rho}\frac{\partial \rho E_c E_w}{\partial x} + E_\alpha\frac{\phi}{\rho}\\
&+ \frac{p}{\rho}\frac{\partial u}{\partial x} + \frac{E_c}{\rho}\frac{\partial \rho E_w}{\partial x} + \frac{E_c^2}{\tau^{(c)}} + E_w w\frac{\partial u}{\partial x} + E_w\frac{\partial E_c}{\partial x} + \frac{E_w}{\rho}\lambda_0\Bigg].
\end{aligned}
\tag{32}
$$

From this equation, after some cancelation, we obtain the desired entropy balance law as

$$
\begin{aligned}
\frac{dS}{dt} &= \frac{1}{T}\left(E_\alpha\frac{\phi}{\rho} + \frac{E_c^2}{\tau^{(c)}} + \frac{E_w}{\rho}\lambda_0\right)\\
&= \frac{1}{T}\left[\frac{(p_1-p_2)^2}{\rho\tau^{(p)}} + \frac{1}{\tau^{(c)}}\left(\mu_1 - \mu_2 + (1-2c)\frac{w^2}{2}\right)^2 + \frac{c^2(1-c)^2w^2}{\rho}\zeta\right].
\end{aligned}
\tag{33}
$$

We observe that the right-hand side in the preceding equation, which represents the entropy production, is always a non-negative quantity.

## 3. EQUATIONS OF STATE

The equations of state we employ in the model for gas–liquid flows, obtained from a linearized form of the Mie–Grüneisen equations [11, 14, 31, 32], are presented here.

The expression for the specific energy is analogous to the expression presented in [14], with the difference of the presence of two constants $\bar{e}_i$ and $s_{0,i}$, introduced here in order to ensure the thermodynamic equilibrium in phase transition problems when the chemical potentials of the two phases are equal [32], and the additional parameter $p_{0,i}$ denoting a reference pressure for the $i$th phase.

With the introduction of these parameters, the specific energy for the $i$th phase can be written in the following way:

$$
e_i(\rho_i, s_i) = \bar{e}_i + c_{v,i}T_{0,i}\left(\frac{\rho_i}{\rho_{0,i}}\right)^{\gamma_i - 1}\exp\left(\frac{s_i - s_{0,i}}{c_{v,i}}\right) + \frac{\rho_{0,i}C_{0,i}^2 - \gamma_i p_{0,i}}{\gamma_i \rho_i},
\tag{34}
$$

where $\bar{e}_i$ is a constant parameter representing the formation energy of the fluid, $c_{v,i}$ is the specific heat capacity at constant volume, $T_{0,i}$ is the reference temperature, $\rho_{0,i}$ is the reference density, $s_{0,i}$ is the entropy at the reference state $(\rho_{0,i}, T_{0,i})$, $C_{0,i}$ is a reference sound of speed at temperature $T_{0,i}$ and $\gamma_i$ is the adiabatic exponent.



DOI: 10.1002/fld

While for a liquid phase, the reference pressure $p_{0,i}$ is given as an independent parameter, for a gas phase, it is defined as

$$p_{0,i} = \frac{\rho_{0,i} C_{0,i}^2}{\gamma_i}, \tag{35}$$

in order to ensure that the last term of equation (34) cancels when dealing with gases.

Now, using the relationships given by equation (2), we obtain the following expressions for the pressure and temperature of the two phases:

$$p_i(\rho_i, s_i) = (\gamma_i - 1)\rho_{0,i} c_{v,i} T_{0,i} \left(\frac{\rho_i}{\rho_{0,i}}\right)^{\gamma_i} \exp\left(\frac{s_i - s_{0,i}}{c_{v,i}}\right) - \frac{\rho_{0,i} C_{0,i}^2 - \gamma_i p_{0,i}}{\gamma_i},$$

$$T_i(\rho_i, s_i) = T_{0,i} \left(\frac{\rho_i}{\rho_{0,i}}\right)^{\gamma_i - 1} \exp\left(\frac{s_i - s_{0,i}}{c_{v,i}}\right).$$

Furthermore, by combining the preceding pressure equation with equation (34), the pressure for both phases can be written as a function of the density and the specific internal energy:

$$p_i(\rho_i, e_i) = (\gamma_i - 1)\rho_i (e_i - \bar{e}_i) - \left(\rho_{0,i} C_{0,i}^2 - \gamma_i p_{0,i}\right). \tag{36}$$

This expression has the same form of the equation of state utilized in [32] for the stiffened gas approximation, and it highlights the contribution of $\bar{e}_i$ to the term $(\gamma_i - 1)\rho_i (e_i - \bar{e}_i)$ in the phase pressure, representing a repulsive effect present in all the media (gas, liquid, and solid) due to the molecular agitation.

We also observe that it is possible to write the energy and the pressure of the two phases in a more convenient form as functions of the densities $\rho_i$ and the common temperature $T$ as

$$e_i(\rho_i, T) = \bar{e}_i + c_{v,i} T + \frac{\rho_{0,i} C_{0,i}^2 - \gamma_i p_{0,i}}{\gamma_i \rho_i}, \tag{37}$$

$$p_i(\rho_i, T) = c_{v,i}(\gamma_i - 1)\rho_i T - \frac{\rho_{0,i} C_{0,i}^2 - \gamma_i p_{0,i}}{\gamma_i}, \tag{38}$$

$$s_i(\rho_i, T) = s_0 + c_{v,i} \ln\left[\frac{T}{T_{0,i}} \left(\frac{\rho_{0,i}}{\rho_i}\right)^{\gamma_i - 1}\right]. \tag{39}$$

Introducing the notation $\bar{p}_i$ for the limit of the pressure of the $i$th phase at absolute zero ($T = 0K$):

$$\bar{p}_i = \frac{\rho_{0,i} C_{0,i}^2 - \gamma_i p_{0,i}}{\gamma_i}, \tag{40}$$

we obtain the more compact form for the specific energy and the pressure:

$$e_i(\rho_i, T) = \bar{e}_i + c_{v,i} T + \frac{\bar{p}_i}{\rho_i}, \tag{41}$$

$$p_i(\rho_i, T) = c_{v,i}(\gamma_i - 1)\rho_i T - \bar{p}_i. \tag{42}$$

The negative term $-\bar{p}_i$ in the equation for pressure represents the effects of the molecular attraction guaranteeing cohesion in the liquid and solid phases, and it is null for gas phases.



DOI: 10.1002/fld

Using the preceding expressions for the specific energy, the pressure, and the specific entropy as functions of the density and the temperature, we find the following expression for the chemical potentials $\mu_i$:

$$\mu_i = \bar{e}_i - Tc_{v,i}\left(\frac{s_{0,i}}{\gamma_i} - \gamma_i + \ln\left[\frac{T}{T_{0,i}}\left(\frac{\rho_{0,i}}{\rho_i}\right)^{\gamma_i - 1}\right]\right) \tag{43}$$

or, in terms of the reference sound speed $C_{0,i}$ instead of the reference temperature $T_{0,i}$:

$$\mu_i = \bar{e}_i - Tc_{v,i}\left(\frac{s_{0,i}}{\gamma_i} - \gamma_i - \ln\left[\frac{Tc_{v_i}\gamma_i(\gamma_i - 1)}{C_{0,i}^2}\left(\frac{\rho_{0,i}}{\rho_i}\right)^{\gamma_i - 1}\right]\right). \tag{44}$$

## 4. CHARACTERISTIC ANALYSIS

In order to find the eigenvalues of the hyperbolic system of equations (23)–(28), we find an equivalent quasilinear form

$$\frac{\partial \mathbf{v}}{\partial t} + B(\mathbf{v})\frac{\partial \mathbf{v}}{\partial x} = \mathbf{Z}(\mathbf{v}), \tag{45}$$

where $\mathbf{v}$ is the vector of primitive variables

$$\mathbf{v} = (\alpha_1, S, \rho_1, \rho_2, u_1, u_2)^T. \tag{46}$$

We remark that with this choice of the vector $\mathbf{v}$, for $0 < \alpha_1 < 1$ and $\rho_i > 0$, it is easy to show that there exists a bijection $\Phi : \mathbf{v} \to \mathbf{q}$.

Now, from the system of equation (16) and the entropy equation (33), the following nonconservative system of equations for the primitive variables can be obtained:

$$\begin{aligned}
\frac{\partial \alpha_1}{\partial t} + u\frac{\partial \alpha_1}{\partial x} &= 0,\\
\frac{\partial S}{\partial t} + u\frac{\partial S}{\partial x} &= \frac{1}{T}\left(\frac{\tau^{(p)}\Omega_1^2}{\rho} + \frac{\tau^{(c)}\Omega_2^2}{\rho^2} + \frac{\rho\Omega_5^2}{\zeta}\right),\\
\frac{\partial \rho_1}{\partial t} + \frac{\alpha_2\rho_2\rho_1}{\alpha_1\rho}(u_1 - u_2)\frac{\partial \alpha_1}{\partial x} + u_1\frac{\partial \rho_1}{\partial x} + \rho_1\frac{\partial u_1}{\partial x} &= -\frac{\rho_1}{\alpha_1\rho}\Omega_1 + \frac{\Omega_2}{\alpha_1},\\
\frac{\partial \rho_2}{\partial t} + \frac{\alpha_1\rho_1\rho_2}{\alpha_2\rho}(u_1 - u_2)\frac{\partial \alpha_1}{\partial x} + u_2\frac{\partial \rho_2}{\partial x} + \rho_2\frac{\partial u_2}{\partial x} &= \frac{\rho_2}{\alpha_2\rho}\Omega_1 - \frac{\Omega_2}{\alpha_2},\\
\frac{\partial u_1}{\partial t} + u_1\frac{\partial u_1}{\partial x} + \frac{1}{\rho_1}\frac{\partial p_1}{\partial x} + \frac{p_1 - p_2}{\rho}\frac{\partial \alpha_1}{\partial x} - c_2(s_1 - s_2)\frac{\partial T}{\partial x} &= \frac{\alpha_2\rho_2}{\rho}\Omega_5 - \frac{u_1 - u_2}{\rho}\Omega_2,\\
\frac{\partial u_2}{\partial t} + u_2\frac{\partial u_2}{\partial x} + \frac{1}{\rho_2}\frac{\partial p_2}{\partial x} + \frac{p_1 - p_2}{\rho}\frac{\partial \alpha_1}{\partial x} + c_1(s_1 - s_2)\frac{\partial T}{\partial x} &= -\frac{\alpha_1\rho_1}{\rho}\Omega_5 - \frac{u_1 - u_2}{\rho}\Omega_2.
\end{aligned} \tag{47}$$

In order to have the system in the desired form (45), we have to express the derivatives $\partial p_i/\partial x$ and $\partial T/\partial x$ as functions of the derivatives of the primitive variables with respect to $x$. We observe that because of the equal phase temperatures, one can derive phase entropies $s_i$ as a function



DOI: 10.1002/fld

of volume fraction $\alpha_1$, phase densities $\rho_i$, and mixture entropy $S$ (i.e., we can explicitly write $s_1 = \tilde{s}_1(\alpha_1, \rho_1, \rho_2, S)$ and $s_2 = \tilde{s}_2(\alpha_1, \rho_1, \rho_2, S)$) by solving the following system of equations:

$$T_1 = \frac{\partial(e_1(\rho_1, s_1))}{\partial s_1} = T, \qquad T_2 = \frac{\partial(e_2(\rho_2, s_2))}{\partial s_2} = T, \qquad \text{and} \qquad c_1 s_1 + c_2 s_2 = S. \tag{48}$$

From the first two equations, solving for $s_1$ and $s_2$, we can find $s_1 = \overline{s}_1(\rho_1, T)$ and $s_2 = \overline{s}_2(\rho_2, T)$. Now, substituting in the last equation and solving for $T$, we can find

$$T = \tilde{T}(\alpha_1, \rho_1, \rho_2, S). \tag{49}$$

Then, we can define $\tilde{s}_1$ and $\tilde{s}_2$ as

$$\tilde{s}_1 = \overline{s}_1(\rho_1, \tilde{T}) \qquad \text{and} \qquad \tilde{s}_2 = \overline{s}_2(\rho_2, \tilde{T}),$$

and, from the equations of state, we can write the phase pressures and the common temperature as

$$\tilde{p}_i(\alpha_1, \rho_1, \rho_2, S) = p_i(\rho_i, \tilde{s}_i),$$
$$\tilde{T}(\alpha_1, \rho_1, \rho_2, S) = T_i(\rho_i, \tilde{s}_i),$$

and their derivatives with respect to $x$ as

$$\frac{\partial T}{\partial x} = \frac{\partial \tilde{T}}{\partial \alpha_1}\frac{\partial \alpha_1}{\partial x} + \frac{\partial \tilde{T}}{\partial \rho_1}\frac{\partial \rho_1}{\partial x} + \frac{\partial \tilde{T}}{\partial \rho_2}\frac{\partial \rho_2}{\partial x} + \frac{\partial \tilde{T}}{\partial S}\frac{\partial S}{\partial x}, \tag{50}$$

$$\frac{\partial p_i}{\partial x} = \frac{\partial \tilde{p}_i}{\partial \alpha_1}\frac{\partial \alpha_1}{\partial x} + \frac{\partial \tilde{p}_i}{\partial \rho_1}\frac{\partial \rho_1}{\partial x} + \frac{\partial \tilde{p}_i}{\partial \rho_2}\frac{\partial \rho_2}{\partial x} + \frac{\partial \tilde{p}_i}{\partial S}\frac{\partial S}{\partial x}. \tag{51}$$

Substituting in the quasilinear system (47), we can finally write the matrix $B(\mathbf{v})$ as

$$B = \begin{bmatrix} u & 0 & 0 & 0 & 0 & 0 \\ 0 & u & 0 & 0 & 0 & 0 \\ b_{3,1} & 0 & u_1 & 0 & \rho_1 & 0 \\ b_{4,1} & 0 & 0 & u_2 & 0 & \rho_2 \\ [5pt] b_{5,1} & b_{5,2} & \dfrac{1}{\rho_1}\dfrac{\partial \tilde{p}_1}{\partial \rho_1} - c_2(s_1 - s_2)\dfrac{\partial \tilde{T}}{\partial \rho_1} & \dfrac{1}{\rho_1}\dfrac{\partial \tilde{p}_1}{\partial \rho_2} - c_2(s_1 - s_2)\dfrac{\partial \tilde{T}}{\partial \rho_2} & u_1 & 0 \\ b_{6,1} & b_{6,2} & \dfrac{1}{\rho_2}\dfrac{\partial \tilde{p}_2}{\partial \rho_1} + c_1(s_1 - s_2)\dfrac{\partial \tilde{p}}{\partial \rho_1} & \dfrac{1}{\rho_2}\dfrac{\partial \tilde{p}_2}{\partial \rho_2} + c_1(s_1 - s_2)\dfrac{\partial \tilde{T}}{\partial \rho_1} & 0 & u_2 \end{bmatrix}, \tag{52}$$

where

$$b_{3,1} = c_2\frac{\rho_1}{\alpha_1}(u_1 - u_2), \tag{53}$$

$$b_{4,1} = c_1\frac{\rho_2}{\alpha_2}(u_1 - u_2), \tag{54}$$

$$b_{5,1} = \frac{p_1 - p_2}{\rho} + \frac{1}{\rho_1}\frac{\partial p_1}{\partial \alpha_1} - c_2(s_1 - s_2)\frac{\partial T}{\partial \alpha_1}, \tag{55}$$



DOI: 10.1002/fld

$$b_{5,2} = \frac{1}{\rho_1}\frac{\partial p_1}{\partial S} - c_2(s_1 - s_2)\frac{\partial T}{\partial S}, \tag{56}$$

$$b_{6,1} = \frac{p_1 - p_2}{\rho} + \frac{1}{\rho_2}\frac{\partial p_2}{\partial \alpha_1} + c_1(s_1 - s_2)\frac{\partial T}{\partial \alpha_1}, \tag{57}$$

$$b_{6,2} = \frac{1}{\rho_2}\frac{\partial p_2}{\partial S} + c_1(s_1 - s_2)\frac{\partial T}{\partial S}, \tag{58}$$

Because of the structure of matrix $B$, the equation for the eigenvalues does not depend on the coefficients $b_{i,j}$ defined in (53–58), and the characteristic polynomial takes the form

$$\pi(\lambda) = (u - \lambda)^2 \cdot \det(A - \lambda I), \tag{59}$$

where matrix $A$ is

$$A = \begin{bmatrix} u_1 & 0 & \rho_1 & 0 \\ 0 & u_2 & 0 & \rho_2 \\ \frac{1}{\rho_1}\frac{\partial \tilde{p}_1}{\partial \rho_1} - c_2(s_1 - s_2)\frac{\partial \tilde{T}}{\partial \rho_1} & \frac{1}{\rho_1}\frac{\partial \tilde{p}_1}{\partial \rho_2} - c_2(s_1 - s_2)\frac{\partial \tilde{T}}{\partial \rho_2} & u_1 & 0 \\ \frac{1}{\rho_2}\frac{\partial \tilde{p}_2}{\partial \rho_1} + c_1(s_1 - s_2)\frac{\partial \tilde{T}}{\partial \rho_1} & \frac{1}{\rho_2}\frac{\partial \tilde{p}_2}{\partial \rho_2} + c_1(s_1 - s_2)\frac{\partial \tilde{T}}{\partial \rho_1} & 0 & u_2 \end{bmatrix}.$$

The characteristic polynomial of $A$ is $\tilde{\pi}(\lambda) = \sum_{i=0}^{4} a_i \lambda^i$, where

$$a_4 = 1,$$

$$a_3 = -(2u_1 + 2u_2),$$

$$a_2 = \left(u_1^2 + u_2^2 + 4u_1u_2 - \frac{\partial \tilde{p}_1}{\partial \rho_1} - \frac{\partial \tilde{p}_2}{\partial \rho_2} - c_1\rho_2(s_1 - s_2)\frac{\partial \tilde{T}}{\partial \rho_2} + c_2\rho_1(s_1 - s_2)\frac{\partial \tilde{T}}{\partial \rho_1}\right),$$

$$a_1 = -\left(2u_1u_2^2 + 2u_1^2u_2 - 2u_2\frac{\partial \tilde{p}_1}{\partial \rho_1} - 2u_1\frac{\partial \tilde{p}_2}{\partial \rho_2} - 2c_1\rho_2u_1(s_1 - s_2)\frac{\partial \tilde{T}}{\partial \rho_2} + 2c_2\rho_1u_2(s_1 - s_2)\frac{\partial \tilde{T}}{\partial \rho_1}\right),$$

$$a_0 = \left(u_1^2u_2^2 - u_2^2\frac{\partial \tilde{p}_1}{\partial \rho_1} - u_1^2\frac{\partial \tilde{p}_2}{\partial \rho_2} - c_1\rho_2u_1^2(s_1 - s_2)\frac{\partial \tilde{T}}{\partial \rho_2} + c_2\rho_1u_2^2(s_1 - s_2)\frac{\partial \tilde{T}}{\partial \rho_1} + \frac{\partial \tilde{p}_1}{\partial \rho_1}\frac{\partial \tilde{p}_2}{\partial \rho_2} - \frac{\partial \tilde{p}_1}{\partial \rho_2}\frac{\partial \tilde{p}_2}{\partial \rho_1} + c_1\rho_2(s_1 - s_2)\frac{\partial \tilde{p}_1}{\partial \rho_1}\frac{\partial \tilde{T}}{\partial \rho_2} - c_1\rho_2(s_1 - s_2)\frac{\partial \tilde{p}_1}{\partial \rho_2}\frac{\partial \tilde{T}}{\partial \rho_1} + c_2\rho_1(s_1 - s_2)\frac{\partial \tilde{p}_2}{\partial \rho_1}\frac{\partial \tilde{T}}{\partial \rho_2} - c_2\rho_1(s_1 - s_2)\frac{\partial \tilde{p}_2}{\partial \rho_2}\frac{\partial \tilde{T}}{\partial \rho_1}\right).$$



DOI: 10.1002/fld

We observe that it is possible to write the characteristic polynomial $\tilde{\pi}(\lambda)$ in the more compact form

$$\tilde{\pi}(\lambda) = \pi_1(\lambda) \cdot \pi_2(\lambda) - \pi_3, \tag{60}$$

where

$$\pi_1(\lambda) = \lambda^2 - 2u_1\lambda + u_1^2 - \frac{\partial \tilde{p}_1}{\partial \rho_1} + c_2\rho_1(s_1 - s_2)\frac{\partial \tilde{T}}{\partial \rho_1},$$
$$\pi_2(\lambda) = \lambda^2 - 2u_2\lambda + u_2^2 - \frac{\partial \tilde{p}_2}{\partial \rho_2} - c_1\rho_2(s_1 - s_2)\frac{\partial \tilde{T}}{\partial \rho_2},$$
$$\pi_3 = \left(\frac{\partial \tilde{p}_2}{\partial \rho_1} + c_1\rho_2(s_1 - s_2)\frac{\partial \tilde{T}}{\partial \rho_1}\right) \cdot \left(\frac{\partial \tilde{p}_1}{\partial \rho_2} - c_2\rho_1(s_1 - s_2)\frac{\partial \tilde{T}}{\partial \rho_2}\right).$$

The coefficient of the characteristic polynomial can be written in terms of the sound speeds $C_i$ and of the partial derivatives of the temperatures, both defined in terms of the original equations of state (1) and (2). Then, once the polynomial is defined, a simple numerical method can be used to find the eigenvalues of the system. More details are given in the Appendix.

### *4.1. Simplified models*

We analyze here the eigenvalues of the Jacobian matrix in some particular case with an additional hypothesis that simplifies the model.

First, we consider the case with a single velocity, that is, $u_1 = u_2 = u$, corresponding to an analytical solution obtained with a relative velocity relaxation ($\lambda_0 = +\infty$). With this assumption, the characteristic polynomial $\tilde{\pi}(\lambda)$ takes the following form:

$$\left[y - \left(\frac{\partial \tilde{P}_1}{\partial \rho_1} - c_2\rho_1(s_1 - s_2)\frac{\partial \tilde{T}}{\partial \rho_1}\right)\right]\left[y - \left(\frac{\partial \tilde{P}_2}{\partial \rho_2} + c_1\rho_2(s_1 - s_2)\frac{\partial \tilde{T}}{\partial \rho_2}\right)\right] - \pi_3, \tag{61}$$

where

$$y = (\lambda - u)^2.$$

Now, from the two solutions $y_1$ and $y_2$ of the second-order polynomial (61), we obtain

$$\lambda_{1,2} = u \pm \sqrt{y_1} \qquad \text{and} \qquad \lambda_{3,4} = u \pm \sqrt{y_2},$$

where the terms $y_1$ and $y_2$ do not depend on the velocities of the two phases. Furthermore, writing the coefficients of the characteristic polynomial in terms of the sound speeds $C_i$ (Appendix), we have that

$$y_1 \to C_1^2 \quad \text{for} \quad \alpha_1 \to 0, \tag{62}$$

$$y_2 \to C_2^2 \quad \text{for} \quad \alpha_1 \to 1. \tag{63}$$

Thus, in the case of a very diluted regime, two eigenvalues approach the usual characteristic velocities associated with the carrier phase, given by the velocity of the phase plus and minus the phase sound speed.

## 5. NUMERICAL SOLUTION OF THE MODEL

For the numerical integration of the system, the fractional-step method presented in [15] is applied by first solving the homogeneous system and then the ODE system where the flux terms are neglected and only the source terms are considered. Using the compact form (16) of the system and



DOI: 10.1002/fld

following the Strang splitting, the fractional-step method results in the solution of the following two subproblems:

$$\begin{array}{l}\text{Problem A: } \mathbf{q}_t + \mathbf{F}(\mathbf{q})_x = 0.\\ \text{Problem B: } \mathbf{q}_t = \boldsymbol{\Omega}(\mathbf{s}).\end{array} \tag{64}$$

### 5.1. Integration of the homogeneous system

Because of the complexity of the equations, the development of exact or approximate Riemann solvers for the homogeneous part of the two-phase single-temperature model can be a difficult task. In particular, the evaluation of the eigenvalues and the eigenvectors of the Jacobian matrix of the fluxes can be very expensive from a computational point of view. For this reason, to solve the hyperbolic homogeneous system of the step A, a so-called Godunov-like central (or central-upwind) scheme formulation is adopted. This family of schemes shares some of the high-resolution properties of classical (approximate) Riemann-solver-based upwind schemes, while being much simpler to implement. In particular, the central finite-volume scheme described in this work is not based on the complete eigenstructure of the Jacobian matrix of the fluxes, and only the numerical fluxes and the maximum and minimum eigenvalues (the largest and smallest roots of the characteristic polynomial $\tilde{\pi}(\lambda)$ given in equation (59)) are requested for its implementation.

As said, the numerical scheme adopted is based on a central-upwind formulation and can be written in the form

$$\mathbf{Q}_i^{n+1} = \mathbf{Q}_i^n - \frac{\Delta t}{\Delta x}\left(\mathbf{F}_{i+\frac{1}{2}} - \mathbf{F}_{i-\frac{1}{2}}\right), \tag{65}$$

where $\mathbf{Q}_i^n$ is an approximation of the average of $\mathbf{q}$ over the $i$th cell at the $n$th time step and $\mathbf{F}_{i+1/2} \approx \mathbf{F}(\mathbf{Q}_{i+1/2})$ is the numerical flux, which is a function of inter-cell boundary value $\mathbf{Q}_{i+1/2}$ evaluated at an intermediate time step $t^{n+1/2}$. The latter can be obtained numerically as a solution of a local Riemann problem. Here, the MUSCL-Hancock method with linear reconstruction and limited slope is used, providing second-order accuracy. Different from [14], the linear reconstruction is performed on a set of primitive variables $\mathbf{U} = (\alpha_1, p_1, p_2, u, w, T)$ instead of on the conservative variables $\mathbf{q}$ to ensure the positivity of densities, energy, and pressures, which is an essential issue in the discretization of the model. With this choice of the vector $\mathbf{U}$, there exists a bijection

$$\mathbf{Q} = \Gamma(\mathbf{U}) = (\Gamma_1(\mathbf{U}), \ldots, \Gamma_6(\mathbf{U})).$$

The reconstruction is obtained as

$$\mathbf{U}_i^{n,L} = \mathbf{U}_i^n - \frac{\Delta x}{2}(\mathbf{U}_i^n)' \qquad \mathbf{U}_i^{n,R} = \mathbf{U}_i^n + \frac{\Delta x}{2}(\mathbf{U}_i^n)', \tag{66}$$

where $(\mathbf{U}_i^n)'$ is an approximation of the first spatial derivative of the solution at the point $x_i$ at the time $t^n$. In order to prevent high derivative values and thus oscillations in the numerical solution, nonlinear slope limiter functions should be adopted. In particular, in this work, the Van-Leer limiter [33] $\varphi_{vl}$ has been used:

$$\begin{aligned}(\mathbf{U}_i^n)' &= \varphi_{vl}(\mathbf{U}_{i-1}^n, \mathbf{U}_i^n, \mathbf{U}_{i+1}^n)\\ &= \begin{cases} \dfrac{2}{\Delta x} \cdot \dfrac{\left(\Delta \mathbf{U}^n_{i+\frac{1}{2}}\right)\left(\Delta \mathbf{U}^n_{i-\frac{1}{2}}\right)}{\Delta \mathbf{U}^n_{i+\frac{1}{2}} + \Delta \mathbf{U}^n_{i-\frac{1}{2}}}, & \text{if } \left(\Delta \mathbf{U}^n_{i+\frac{1}{2}}\right)\left(\Delta \mathbf{U}^n_{i-\frac{1}{2}}\right) > 0\\ 0 & \text{otherwise}\end{cases},\end{aligned} \tag{67}$$

where

$$\Delta \mathbf{U}^n_{i+\frac{1}{2}} = \mathbf{U}^n_{i+1} - \mathbf{U}^n_i \qquad \Delta \mathbf{U}^n_{i-\frac{1}{2}} = \mathbf{U}^n_i - \mathbf{U}^n_{i-1}.$$

A schematic illustration of a linear reconstruction is reported in Figure 1. Then, from the reconstructed interface values of the primitive variables, the corresponding values of the characteristic



DOI: 10.1002/fld

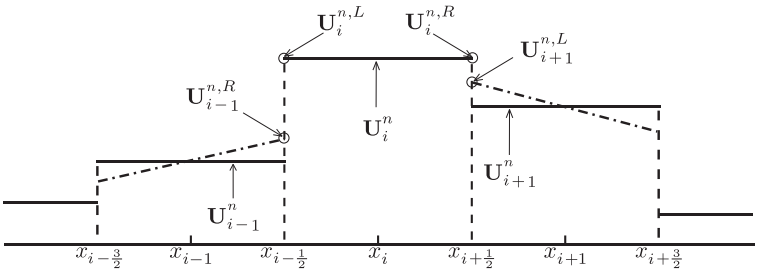


Figure 1. Schematic illustration of a linear reconstruction. The solid line corresponds to the average integral $\mathbf{U}_i^n$ in the $i$th cell, while the dash-dotted line represents the linear reconstruction inside the $i$th cell.

variables $\mathbf{Q}_i^{n,L} = \Gamma(\mathbf{U}_i^{n,L})$ and $\mathbf{Q}_i^{n,R} = \Gamma(\mathbf{U}_i^{n,R})$ are obtained. These boundary extrapolated values are evolved in time by

$$\widetilde{\mathbf{Q}}_i^{n+1/2,L} = \mathbf{Q}_i^{n,L} - \frac{1}{2}\frac{\Delta t}{\Delta x}\left(\mathbf{F}\left(\mathbf{Q}_i^{n,R}\right) - \mathbf{F}\left(\mathbf{Q}_i^{n,L}\right)\right), \tag{68}$$

$$\widetilde{\mathbf{Q}}_i^{n+1/2,R} = \mathbf{Q}_i^{n,R} - \frac{1}{2}\frac{\Delta t}{\Delta x}\left(\mathbf{F}\left(\mathbf{Q}_i^{n,R}\right) - \mathbf{F}\left(\mathbf{Q}_i^{n,L}\right)\right). \tag{69}$$

Finally, using as initial value $\widetilde{\mathbf{Q}}_i^{n+1/2,L}$ and $\widetilde{\mathbf{Q}}_i^{n+1/2,R}$, we integrate the source terms to find the values $\hat{\mathbf{Q}}_i^{n+1/2,L}$ and $\hat{\mathbf{Q}}_i^{n+1/2,R}$ used to evaluate the numerical fluxes $\mathbf{F}_{i+1/2}$ of the finite-volume scheme (65).

The numerical fluxes adopted here are obtained from a modification of the Kurganov, Noelle, and Petrova semidiscrete scheme proposed in [34]. These numerical fluxes, which have been studied in [15], are defined as follows:

$$\mathbf{F}_{i+\frac{1}{2}} = \frac{a^+_{i+\frac{1}{2}}\mathbf{F}\left(\hat{\mathbf{Q}}_{i+1}^{n+1/2,L}\right) - a^-_{i+\frac{1}{2}}\mathbf{F}\left(\hat{\mathbf{Q}}_i^{n+1/2,R}\right)}{a^+_{i+\frac{1}{2}} - a^-_{i+\frac{1}{2}}} - \frac{a^+_{i+\frac{1}{2}}a^-_{i+\frac{1}{2}}}{a^+_{i+\frac{1}{2}} - a^-_{i+\frac{1}{2}}}\left(\hat{\mathbf{Q}}_i^{n+1/2,R} - \hat{\mathbf{Q}}_{i+1}^{n+1/2,L}\right). \tag{70}$$

The speeds $a^+_{i+\frac{1}{2}}$ and $a^-_{i+\frac{1}{2}}$ are the maximum left-going and right-going characteristic speeds at the interface, computed as

$$\begin{aligned} a^+_{i+\frac{1}{2}} &= \max\left(\lambda^{\max}_{i+\frac{1}{2},R}, \lambda^{\max}_{i+\frac{1}{2},L}, 0\right), \\ a^-_{i+\frac{1}{2}} &= \min\left(\lambda^{\min}_{i+\frac{1}{2},R}, \lambda^{\min}_{i+\frac{1}{2},L}, 0\right), \end{aligned} \tag{71}$$

where $\lambda^{\max}_{i+\frac{1}{2},R}$ and $\lambda^{\max}_{i+\frac{1}{2},L}$ are the maximum eigenvalues and $\lambda^{\min}_{i+\frac{1}{2},R}$ and $\lambda^{\min}_{i+\frac{1}{2},L}$ the minimum eigenvalues of the Jacobian matrix of the fluxes evaluated respectively at $\hat{\mathbf{Q}}_{i+1}^{n+1/2,L}$ and $\hat{\mathbf{Q}}_i^{n+1/2,R}$.

### *5.2. Integration of the source terms*

After the integration of the homogeneous hyperbolic system of PDEs defined by problem A, the system of ODEs associated with problem B in the Strang splitting is solved. Using a segregated approach, in [15], it has been shown that the pressure and velocity relaxation terms can be integrated analytically, under the condition of constant pressure relaxation parameter $\tau^{(p)}$ and frictional coefficient $\zeta$. Here, instead, we focus the attention on the numerical integration of the phase exchange relaxation term.



DOI: 10.1002/fld

For the applications presented in this paper, we consider the gas phase being exactly the vapor phase of the liquid, and we assume the characteristic times of phase pressures and velocities equalizing to be negligible compared with the characteristic time of phase transition, and thus the pressure and the velocity relaxations are instantaneous ($\tau^{(p)} = 0$ and $\zeta = +\infty$). With these assumptions, the equations for the integration of the source terms of the volume fraction and the mass fraction of the first phase and the equation of the relative velocity become

$$p_2 - p_1 = 0, \tag{72}$$

$$\frac{\partial q_3}{\partial t} = -\frac{\rho}{\tau^{(c)}}\left(\mu_1 - \mu_2\right), \tag{73}$$

$$w = 0. \tag{74}$$

According to the sign of the difference of the Gibbs free energies, it is possible to have evaporation or condensation, and the reaction ends when the difference becomes zero. Thus, the equilibrium density of the liquid phase (or gas phase) is the density that we have when the difference of the Gibbs energies is zero. Furthermore, we define the relaxation time $\tau^{(c)}$ as a nonlinear function of the temperature:

$$\tau^{(c)} = \tau^{(c),0} + \left|K_T \frac{T - T_{eq}}{T_{eq}}\right|^n \cdot \left|K_p \frac{p - p_{eq}}{p_{eq}}\right|^m, \tag{75}$$

where $\tau^{(c),0}$ is a reference relaxation time, $T_{eq}$ and $p_{eq}$ are the critical temperature and pressure that we have at the thermodynamical equilibrium when the condition given by equations (72) and (74) are satisfied, and $K_T, K_p, n$, and $m$ are empirical parameters measuring the degree of nonlinearity. These are introduced to better model the fact that the transition only occurs in the neighborhood of the critical values of temperature and pressure, when we are close to the thermodynamic equilibrium and the difference of the Gibbs energies is zero. The values of the four constants $K_T, K_p, n$, and $m$ are not obtained directly from the available experimental data, our goal here being to demonstrate only that the kinetic approach can give reasonable results in phase transition modeling.

We show here that it is possible to derive, when the two conditions (72) and (74) hold, an expression of the source term for the mass fraction of the first phase as a function of $q_1$ only.

First of all, we observe that from equation (37), it is possible to write the chemical potential $\mu_i$ as a function of the density $\rho_i$ and the common temperature $T$ only. Now, substituting the expressions for the specific energies in the total energy $q_6$, we obtain the following expression for the temperature $T$:

$$T = \frac{q_6 - \frac{1}{2}\left[q_3 u_1^2 + (q_1 - q_3)u_2^2\right] - q_3\bar{e}_1 - \alpha_1\bar{p}_1 - (q_1 - q_3)\bar{e}_2 - (1-\alpha_1)\bar{p}_2}{q_3 c_{v,1} + (q_1 - q_3)c_{v,2}} \tag{76}$$

where $q_1$ and $q_6$ are constant during the integration of equation (73).

We also observe that the velocities of the two phases, appearing in the expression of the temperature, can be expressed as functions of the conservative variables in the following way:

$$u_1 = \frac{q_4 + q_5(q_1 - \alpha_1\rho_1)}{q_1}, \tag{77}$$

$$u_2 = \frac{q_4 - \alpha_1\rho_1 q_5}{q_1}. \tag{78}$$



DOI: 10.1002/fld

If we assume now that the relative motion of phases can be neglected, then the conservative variable $q_5$ can be set to zero. With this assumption, also the velocities $u_1 = u_2 = q_4/q_1$ are constant during the integration of equation (73), and the equation for the temperature becomes

$$T = \frac{q_6 - \frac{1}{2}\frac{q_4^2}{q_1} - q_3\bar{e}_1 - \alpha_1\bar{p}_1 - (q_1 - q_3)\bar{e}_2 - (1-\alpha_1)\bar{p}_2}{q_3 c_{v,1} + (q_1 - q_3)c_{v,2}}, \tag{79}$$

where the only variables changing during the integration of the phase relaxation term are $q_3$ and $\alpha_1$.

Now, using the condition on the local pressures given by equation (72) for the thermodynamic equilibrium, and the expressions for the pressures from the equations of state defined in terms of the densities and the temperature, we have

$$\rho_1(\gamma_1 - 1)c_{v,1}T - \bar{p}_1 = \rho_2(\gamma_2 - 1)c_{v,2}T - \bar{p}_2. \tag{80}$$

Using the definition of the variable $q_3$ and the conservation of the mixture density $q_1 = \rho$, we can write the density of the two phases as functions of the constant variable $q_1$ and the two variables $q_3$ and $\alpha_1$:

$$\rho_1 = \frac{q_3}{\alpha_1}, \qquad \rho_2 = \frac{q_1 - q_3}{1 - \alpha_1}, \tag{81}$$

and substituting these expressions into equation (80), we obtain

$$T = \frac{\alpha_1(1-\alpha_1)(\bar{p}_1 - \bar{p}_2)}{(1-\alpha_1)q_3(\gamma_1 - 1)c_{v,1} - \alpha_1(q_1 - q_3)(\gamma_2 - 1)c_{v,2}}. \tag{82}$$

Again, as for the other expressions of the mixture temperature given by equation (79), the only variables changing during the integration of the phase relaxation term are $q_3$ and $\alpha_1$, and from the equations (79) and (82), we obtain

$$\frac{q_6 - \frac{1}{2}\frac{q_4^2}{q_1} - q_3\bar{e}_1 - \alpha_1\bar{p}_1 - (q_1 - q_3)\bar{e}_2 - (1-\alpha_1)\bar{p}_2}{q_3 c_{v,1} + (q_1 - q_3)c_{v,2}} = \frac{\alpha_1(1-\alpha_1)(\bar{p}_1 - \bar{p}_2)}{(1-\alpha_1)q_3(\gamma_1 - 1)c_{v,1} - \alpha_1(q_1 - q_3)(\gamma_2 - 1)c_{v,2}} \tag{83}$$

From this one, we can make explicit $\alpha_1$ as a function of $q_3$

$$\alpha_1 \equiv \alpha_1(q_3) \tag{84}$$

and substituting (84) in (79) or (82) and the first of equation (81), we finally have the temperature and the density as $T = T(q_3)$ and $\rho_1 = \rho_1(q_3)$, respectively, and from the equations of state, we can write also the chemical potential $\mu_1$ in terms of $q_3$ only. Furthermore, from equation (81) and the conservation of the mixture density, also $\rho_2$ can be written as function of $q_3$, and consequently $\mu_2$. Thus, under the assumptions of negligible relative velocity and small characteristic time of pressure relaxation compared with that of phase transition, the difference of the chemical potentials in the right-hand side of equation (73) can be written as a function of the conservative variable $q_3$ only.

In order to find an expression for the relaxation time $\tau^{(c)}$, we have to find the critical temperature and thus, the temperature being a function of $q_3$ only during the integration of the phase change term, the equilibrium value $q_3^{eq}$. This value can be evaluated by imposing the condition $\mu_2 - \mu_1 = 0$, from which we obtain an equation in the only unknown $q_3$. The solution can be easily computed using an iterative method like bisection or Newton method, and then, using equations (84) and (81), we also obtain the equilibrium volumetric fraction $\alpha_1$ and density $\rho_1$.



DOI: 10.1002/fld

Once we have the equilibrium values, all the terms of the right-hand side of equation (73) are defined as a function of the integration variable $q_3$. A second-order Cranck–Nicolson method has been applied in this work to integrate the ODE and to update the value of $q_3$:

$$q_3^{(n+1)} = q_3^{(n)} - \frac{\rho\Delta t}{2}\left[\left(\frac{\mu_1\mu_2}{\tau^{(c)}}\right)^{(n)} + \left(\frac{\mu_1\mu_2}{\tau^{(c)}}\right)^{(n+1)}\right]. \tag{85}$$

Now, because of the assumptions of negligible relative velocity and characteristic time of pressure relaxation, all the other conservative variables are constant during the integration except $q_2$. But, substituting the updated value $q_3^{(n+1)}$ in equation (84), the new value of $\alpha_1^{(n+1)}$ is found and also $q_2$ can be updated as $q_2^{(n+1)} = \alpha_1^{(n+1)} q_1$.

## 6. NUMERICAL TESTS

In this section, we solve numerically three test problems in order to investigate the effects of the evaporation term on the single-temperature two-phase model. Each of the test problems represents a Riemann problem for a liquid/gas mixture with instantaneous pressure and velocity relaxations. In the first test, we study the 1D cavitation tube problem presented in [12] and studied in [35, 36], analyzing the effects of the evaporation, with both instantaneous and finite-rate relaxation. Then, as a second test, we present a multidimensional cavitation problem: the cavitating Richtmyer–Meshkov instability test described in [17, 18]. For this test, evaporation is not taken into account, and a small fraction of gas is initially present in the liquid. Finally, we present another multidimensional test, in which the evaporation is considered: the laser-induced cavitation problem [19]. For the 2D tests, a new solver for the parallel open-source CFD software package OpenFOAM has been developed and used, implementing the numerical scheme described in the previous section.

For all the runs presented in this paper, the fractional-step method illustrated in Section 5 has been adopted.

### *6.1. One-dimensional cavitation tube*

In this first test, we consider an evaporation problem for a tube initially at atmospheric pressure and at a temperature of 355 K, filled with water and a small volumetric fraction of water vapor. In this test, the water cannot be treated as pure, and evaporation only occurs if the pressure of the liquid phase is lower than the saturation pressure.

The initial condition is similar to the two-phase expansion tube test described in [12], where a seven-equation model for two-phase flows is applied to model evaporation of metastable liquids. The left part of the tube is set to motion with a velocity of $u_l = -2$ m/s, while the right part is set to motion with a velocity of $u_r = 2$ m/s. In such situation, the pressure, density, and internal energy decrease across the rarefaction waves in order that the velocity reaches zero at the center of the domain. The pressure decreases until the saturation pressure at the local temperature is reached. Then the mass transfer appears, a part of liquid become gas, and the flow becomes a two-phase mixture. This problem has been studied also in [37] in a simplified situation where a small fraction of gas is initially present in the liquid (1% gas by volume) and the mass transfer is not considered. Here, we analyze the effects of different values of the phase exchange term, in order to compare our results with both those presented in [37] and [12].

Indexes 1 and 2 for this application are referred to the parameters of state of water vapor and water, respectively, and the constants for the equations of state are given in Table I. The computational domain considered is $x \in [0, 1]$ (in meters) with the Riemann problem being defined with the interface located at $x = 0.5$. The initial data are given by

- Left: $\alpha_1 = 0.99$, $\alpha_2 = 0.01$, $u_1 = u_2 = -2$ m/s, $p_1 = p_2 = 10^5$ Pa, and $T = 355$ K.
- Right: $\alpha_1 = 0.99$, $\alpha_2 = 0.01$, $u_1 = u_2 = +2$ m/s, $p_1 = p_2 = 10^5$ Pa, and $T = 355$ K.

In Figures 2–4, we present the results of several simulations performed with no evaporation, instantaneous evaporation, and finite-rate evaporation. We observe that for all the tests, the



DOI: 10.1002/fld

Table I. Parameters of state for water and water vapor for the cavitation tube test (from www.engineeringtoolbox.com).

| | $p_0$ (Pa) | $\rho_0$ (kg/m$^3$) | $\gamma$ | $C_0$ (m/s) | $c_v$ (J/(kg· K)) | $\bar{e}$ (J/kg) | $s_0$ |
|---|---|---|---|---|---|---|---|
| Water | $10^5$ | 958.4 | 2.514 | 1542.98 | 1677 | −1.167e+6 | 1307 |
| Vapor | $10^5$ | 0.527 | 1.324 | 501.37 | 1571 | 2.030e+6 | 7742 |

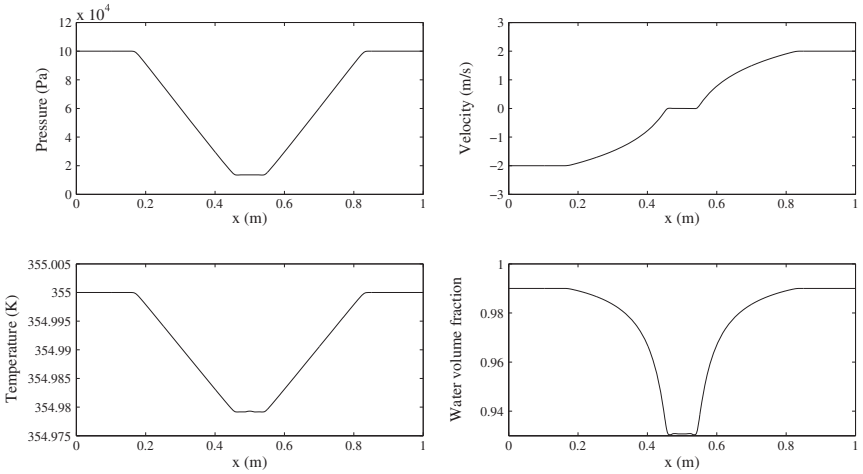


Figure 2. Cavitation tube: mixture pressure (top left), mixture velocity (top right), common temperature (bottom left), and liquid water volume fraction (bottom right) at $t = 3.2 \cdot 10^{-3}$ s computed on 2000 cells for $\tau^{(c)} = +\infty$ (no evaporation). The CPU time is 850 s.

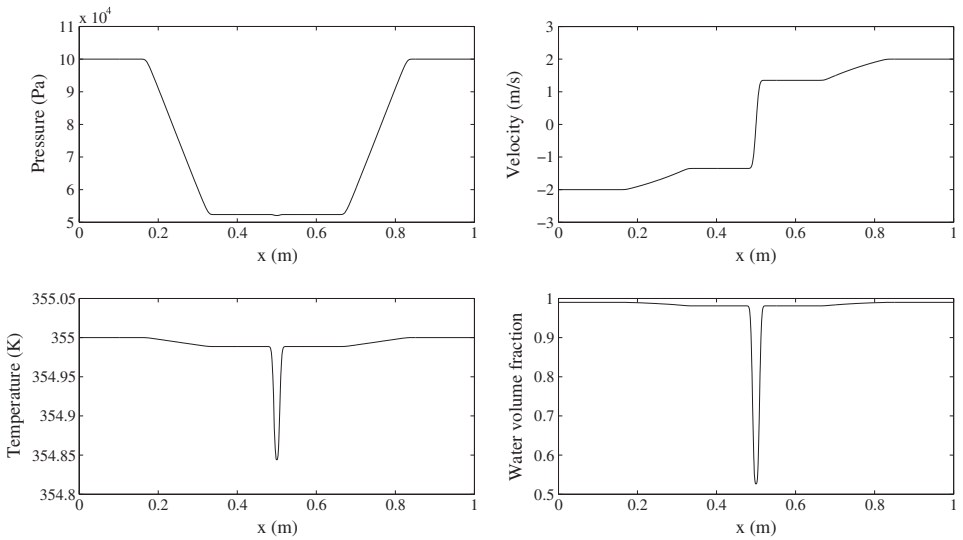


Figure 3. Cavitation tube: mixture pressure (top left), mixture velocity (top right), mixture temperature (bottom left), and liquid water volume fraction (bottom right) at $t = 3.2 \cdot 10^{-3}$ s computed on 2000 cells for $\tau^{(c)} = +0$ (instantaneous evaporation). The CPU time is 1046 s.

magnitude of the temperature variations is small compared with the absolute value of the temperature; therefore, the single-temperature approximation is appropriate.

In Figure 2, the solution for a test without evaporation ($\tau^{(c)} = +\infty$), but with instantaneous pressure and velocity relaxations, is shown at $t = 3.2 \times 10^{-3}$ s. Two symmetric rarefaction waves



DOI: 10.1002/fld

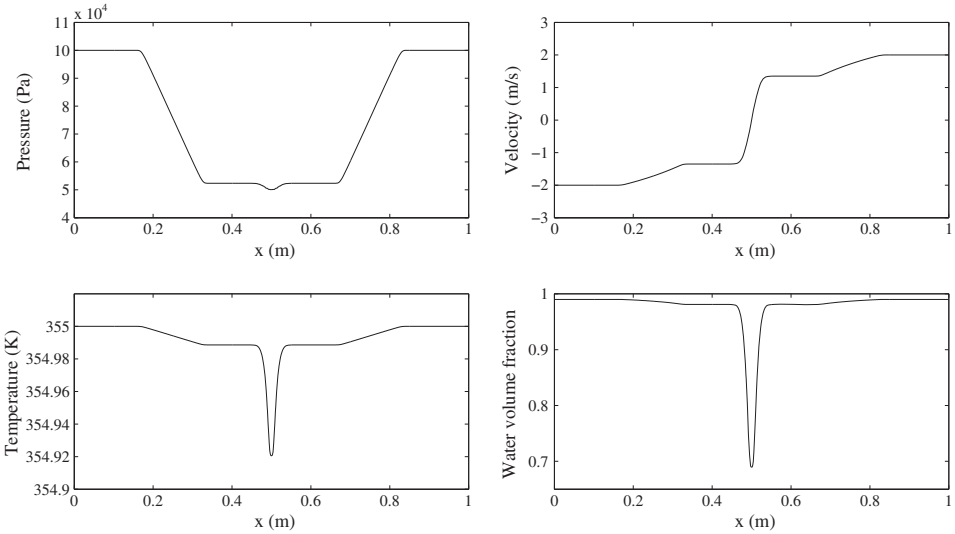


Figure 4. Cavitation tube: mixture pressure (top left), mixture velocity (top right), mixture temperature (bottom left), and liquid water volume fraction (bottom right) at $t = 3.2 \cdot 10^{-3}$ s computed on 2000 cells for $\tau^{(c),0} = 10^5$, $K_T = K_p = 20$, $n = m = 3$ (finite-rate evaporation). The CPU time is 1176 s.

propagate to the left and to the right. At the middle of the domain, the mixture velocity is zero, and the gas volumetric fraction increases because of the expansion. The solution is not physically correct because the expansion wave makes the liquid thermodynamic state metastable and evaporation should occur. These effects are taken into account in the second test, where $\tau^{(c)} = 0$.

The solution at $t = 3.2 \times 10^{-3}$ s of a test with instantaneous pressure and velocity relaxations and evaporation is presented in Figure 3. The solution consists of four rarefaction waves: two waves propagate into the mixture on both sides of the initial velocity discontinuity and two evaporation fronts propagate into the metastable region. These four waves are evident in the two symmetric drops in the temperature and water volume fraction plots.

Finally, in Figure 4, the solution at $t = 3.2 \times 10^{-3}$ s for a test with instantaneous pressure and velocity relaxations and evaporation occurring with finite speed is shown ($\tau^{(c),0} = 10^5$, $K_T = K_p = 20$, $n = m = 3$). In Figure 5, the solutions obtained with instantaneous evaporation (solid line) and without evaporation (dashed line) are compared with the solution obtained with finite-rate evaporation ($\tau^{(c),0} = 10^6$, $K_T = K_p = 20$, $n = m = 3$). We observe that, in order to better highlight the effects of the finite-rate mass transfer and the differences with the instantaneous evaporation test, a larger evaporation rate has been used with respect to the test represented in Figure 4. In all the cases, the gas volume fraction at the center of the tube increases because of rarefaction waves and pressure relaxation. From the plot of the liquid-phase volumetric fraction, we can see that, with a finite-rate evaporation, the evaporation front becomes less sharp. When the phase change occurs, a larger amount of water vapor is present and free to expand, decreasing the volume of the liquid phase and increasing its density. Furthermore, for the finite-rate evaporation, we see that while in the density and volume fraction plots, it is still possible to identify the transition from the expansion waves to the evaporation waves, the velocity profile is more smooth.

As a final plot, to better appreciate the validity and the performance of the method, we also present in Figure 6 the pressure and the water volume fraction at $t = 1.5 \cdot 10^{-3}$ s, obtained when the value of the initial velocities is increased to $-100$ m/s on the left and 100 m/s on the right for a test with instantaneous pressure and velocity relaxations and instantaneous evaporation. With this initial conditions, as shown in [12], four expansion waves are clearly visible.

Comparing the results of this test case with those reported in [12] for a finer grid, we can conclude that a reasonable agreement with their solutions is achieved.



DOI: 10.1002/fld

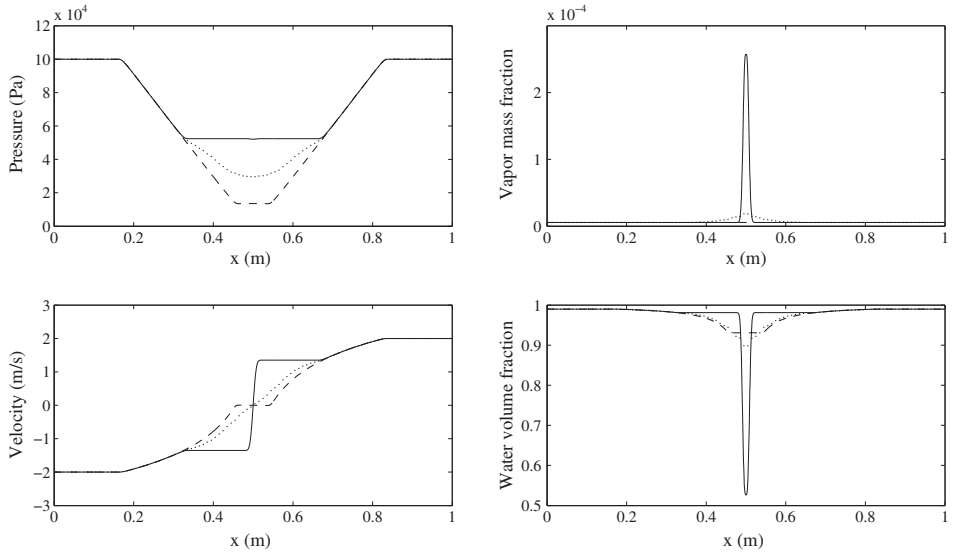


Figure 5. Cavitation tube: mixture pressure (top left), vapor mass fraction (top right), mixture velocity (bottom left), and liquid water volume fraction (bottom right) at $t = 3.2 \cdot 10^{-3}$ s computed on 2000 cells for no evaporation (dashed line), instantaneous evaporation (solid line), and finite-rate evaporation ($\tau^{(c),0} = 10^6$, $K_T = K_p = 20$, $n = m = 3$, dotted line).

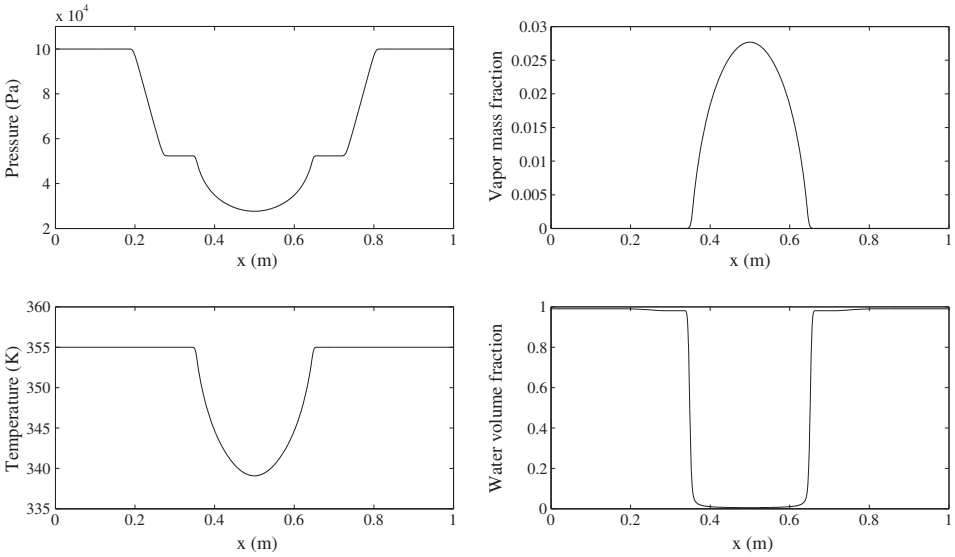


Figure 6. Cavitation tube: mixture pressure (top left), vapor mass fraction (top right), mixture temperature (bottom left), and liquid water volume fraction (bottom right) at $t = 1.5 \cdot 10^{-3}$ s computed on 2000 cells for instantaneous evaporation, pressure relaxation, and velocity relaxation and $u_l = -100$ m/s and $u_r = 100$ m/s. The CPU time is 551 s.

### *6.2. Cavitating Richtmyer–Meshkov instability*

As a second test, we present the 2D gas–water cavitating Richtmyer–Meshkov instability problem proposed in [17, 18]. For this test, the mass transfer is not taken into account, while instantaneous pressure and velocity relaxations are assumed. Indexes 1 and 2 for this application are referred to the parameters of state of water and gas, respectively. Their values are given in Table II and are chosen in agreement with those used in [17].



DOI: 10.1002/fld

Table II. Parameters of state for water and gas for the cavitating Richtmyer–Meshkov instability.

| | $p_0$ (Pa) | $\rho_0$ (kg/m$^3$) | $\gamma$ | $C_0$ (m/s) | $c_v$ (J/(kg·K)) | $\bar{e}$ (J/kg) | $s_0$ |
|---|---|---|---|---|---|---|---|
| Water | $10^5$ | 1000.0 | 4.4 | 1624.94 | 951.0 | 0 | −43,497.97 |
| Gas | $10^5$ | 100.0 | 1.4 | 37.4165 | 714.0 | 0 | −2035.43 |

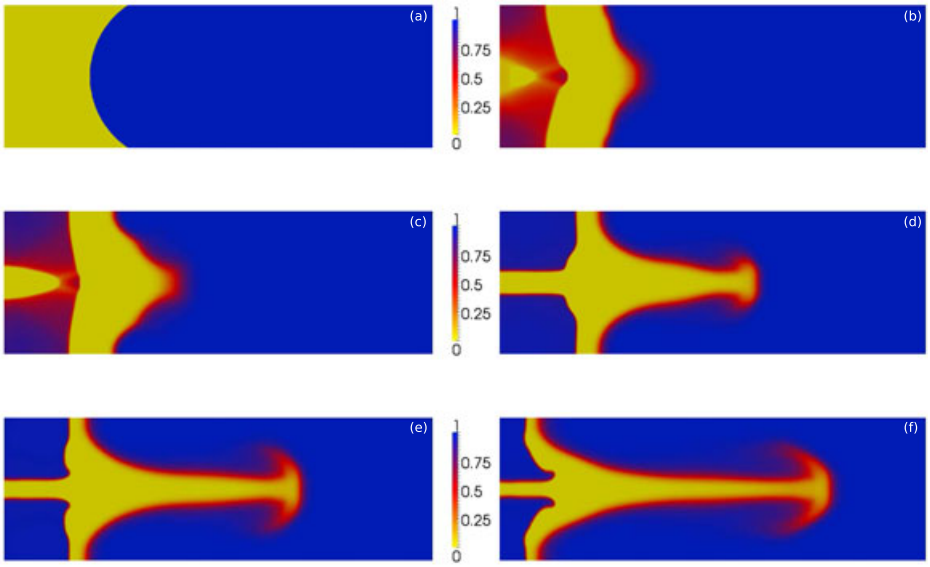


Figure 7. Richtmyer–Meshkov instability: pseudo-color images of gas volume fraction. The results are taken respectively at time $t = 0$ (a), 2.0 (b), 3.1 (c), 6.4 (d), 8.6 (e), and 11.0 ms (f). The solution has been computed using a grid of $1200 \times 400$ cells.

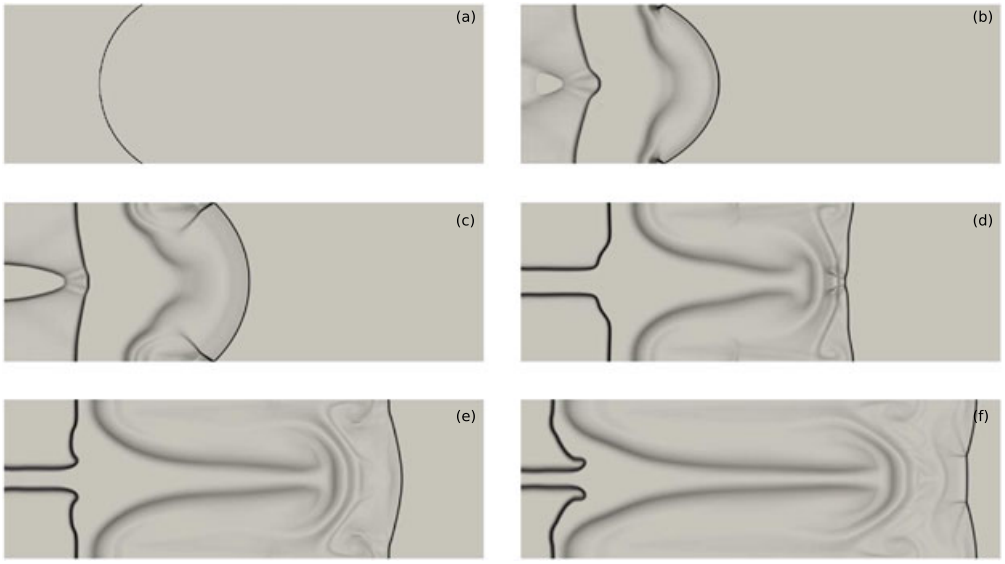


Figure 8. Richtmyer–Meshkov instability: emulated Schlieren image generated from the numerical results plotting $|\nabla\rho|$ in a nonlinear gray map. The results are taken respectively at time $t = 0$ (a), 2.0 (b), 3.1 (c), 6.4 (d), 8.6 (e), and 11.0 ms (f). The solution has been computed using a grid of $1200 \times 400$ cells.



DOI: 10.1002/fld

Table III. Parameters of state for water and water vapor for the laser-induced cavitation problem.

| | $p_0$ (Pa) | $\rho_0$ (kg/m$^3$) | $\gamma$ | $C_0$ (m/s) | $c_v$ (J/(kg· K)) | $\bar{e}$ (J/kg) | $s_0$ |
|---|---|---|---|---|---|---|---|
| Water | $10^5$ | 998.2 | 2.514 | 1374.53 | 1676.97 | −1.200e+6 | 243 |
| Vapor | $10^5$ | 0.527 | 1.324 | 501.37 | 1571.00 | 2.030e+6 | 7742 |

For this test, a rectangular domain $(x, y) \in [0, 3] \times [0, 1]\, m^2$ is considered, where the left part is filled with nearly pure water ($\alpha_2 = 10^{-6}$) and the right part with nearly pure gas ($\alpha_1 = 10^{-6}$). The two phases are separated by a curved interface, a portion of circle with a 0.6 -m radius centered at $x = 1.2$ m, $y = 0.5$ m. Figure 7(a) shows the computational domain and the initial gas–water interface. The top, bottom, and left boundaries are assumed as solid walls, while the right side is considered an outflow boundary. Both liquid and gas phases have an initial velocity of $u_x = -200$ m/s. Furthermore, the initial pressure is set to $10^5$ Pa for both phases, while the temperature profile is chosen in a way that the density of water in the right zone is $\rho_1 = 1000\,\text{kg/m}^3$ and the density of the gas in the left region is $\rho_2 = 100\,\text{kg/m}^3$.

For this test, we use a grid of $1200 \times 400$ cells, and the simulation has been performed on a high-performance computing 48 multicore shared-memory system, using 32 cores. The numerical results are reported in Figures 7 and 8. In Figure 7, we report the gas volume fraction, while in Figure 8, the emulated Schlieren photographs generated from the numerical results plotting $|\nabla\rho|$ in a non–linear gray map are presented. The solutions illustrated in these figures are taken respectively at time $t = 0$ (a), 2 (b), 3.1 (c), 6.4 (d), 8.4 (e) and 11.0 ms (f). From the plots, we can observe that, when the flow impacts the left wall, a right-going shock wave propagates through the curved gas–water interface, producing a Richtmyer–Meshkov instability. This is characterized by expansion waves and an elongating jet. These expansion waves result in a decrease of pressure in the upper and lower corners of the left side of the domain, generating cavitation pockets in these regions. Our results agree well with the ones shown in [17], by looking at the global features of the solution structure. Comparing the plot of the gas volume fraction presented in Figure 7 with the results obtained in [18], we can see that our solution seems to be more diffusive in the resolution of the interfaces between the phases. We have also to remark that the parameters for the equations of state used in [18] are different from those used in [17], thus leading to different characteristic speeds and different propagations of the shock waves.

### *6.3. Laser-induced cavitation-bubble problem*

The last numerical test we present in this work is a numerical simulation for a 2D laser-induced cavitation-bubble problem, where instantaneous evaporation is considered. Many studies related to this problem are dedicated to medical applications, especially in ophthalmology [38–41] and biomedicine.

As a test case, we considered here the laser-induced cavitation-bubble experiments as described in [19]. A laser pulse is focused for a short time into the liquid, producing an increase of the pressure and temperature. Because of the high pressure gradient, a shock wave propagates, causing an expansion and a strong decrease of the pressure in the area previously irradiated by the laser and therefore the evaporation of the liquid. Then the gas bubble generated by the evaporation starts to expand, and after a certain time, owing to the high pressure of the surrounding water, the expansion ends and the bubble begins to collapse. Finally, when the bubble collapses entirely, a new shock wave is generated.

For the numerical simulation, as an initial condition, we consider a square domain $[-5, 5] \times [-5, 5]\,\text{mm}^2$ that contains nearly pure water ($\alpha_2 = 10^{-6}$, where indexes 1 and 2 refer to water and vapor, respectively) at ambient pressure and temperature. The parameters of state for the liquid and gas phases are given in Table III. The zone irradiated by a laser pulse of 0.2 mJ is a sphere whose center is located at $(x, y) = (0, 0)$ with a radius of $5 \times 10^{-2}$ mm. Furthermore, we assume that the pulse is so short in time that the energy is transferred to water instantaneously, resulting, in the zone



DOI: 10.1002/fld

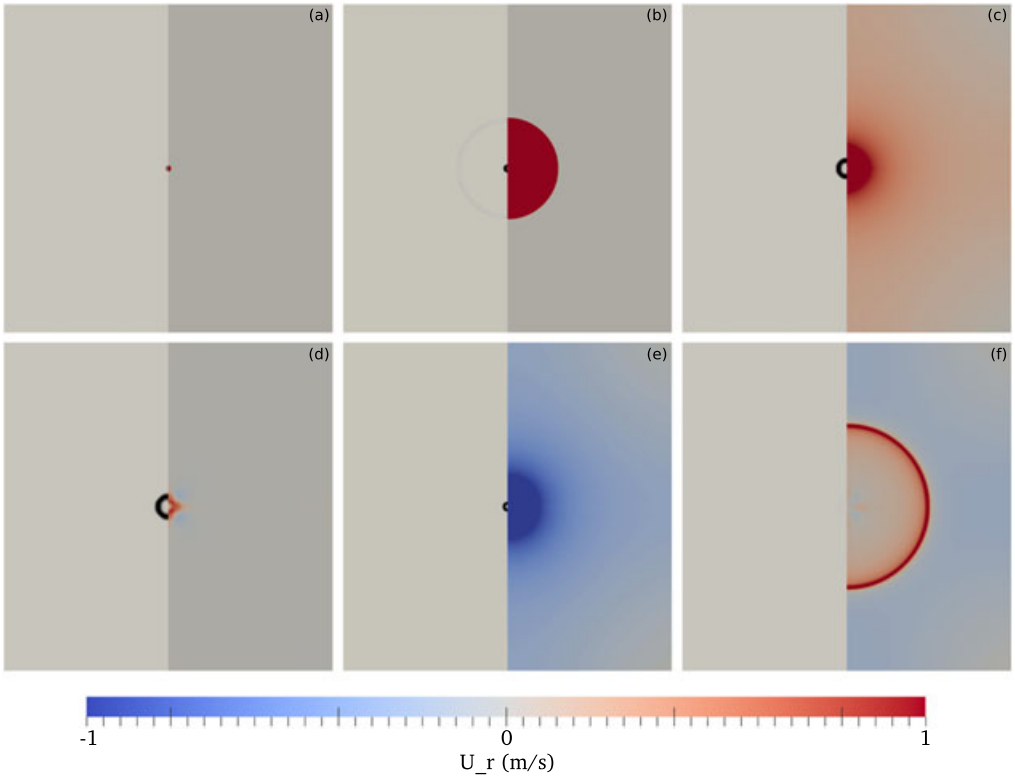


Figure 9. Laser-induced cavitation bubble: emulated Schlieren image generated from the numerical results plotting $|\nabla\rho|$ (left side of each panel) and radial velocity (right side of each panel). The radial velocities greater or equal to 1 m/s are represented by the same red color, while those smaller or equal to $-1$ m/s by the same blue one. The results are taken respectively at time $t = 0.01$ (a), 1.0 (b), 30.0 (c), 75.0 (d), 145.0 (e), and 150.0 $\mu$s (f). The solution has been computed using a grid of $1000 \times 1000$ cells.

irradiated by the laser, in an increase of the pressure up to $\approx 5.8 \times 10^8$ Pa and of the temperature up to $\approx 520$ K.

The results of a numerical simulation, obtained with a $1000 \times 1000$-cell grid, with instantaneous pressure and velocity relaxation, that is, single pressure and temperature, are presented in Figure 9. On the left side of each panel is presented an emulated Schlieren image generated from the numerical results plotting $|\nabla\rho|$, and on the right side, the radial velocity is plotted, in order to distinguish the expanding and collapsing regions. Figure 9(a) illustrates the solution a few instants after the laser pulse ($t = 0.01\,\mu$s). In Figure 9(b), in contrast, we can observe the solution at time $t = 1\,\mu$s. Here, we can see the spherical shock wave that propagates into water and, at the center of the domain, the bubble nucleated due to the cavitation. Furthermore, the positive radial velocity indicates that the bubble is expanding. In Figure 9(c) ($t = 30\,\mu$s), the shock wave exited from the computational domain, but we can see the bubble growth with respect to Figure 9(b). The positive radial velocity around the surface of the bubble indicates that it is still expanding. The maximum radius of the bubble is reached at time $t = 75\,\mu$s, as illustrated in Figure 9(d). Here, we can see that, although the radial velocity inside the bubble is still positive, the water outside the bubble, owing to the high pressure, is starting to move toward the center of the domain. Because of that, the bubble expansion ends, and from now on, the bubble starts to collapse. In Figure 9(e), ($t = 145\,\mu$s), we can observe that the radius of the bubble is decreased, and the negative radial velocity indicates that the bubble will continue to compress until it entirely collapses. The collapse of the bubble produces an increase in pressure at the center of the domain, generating again a shock wave. Because of the lower intensity of the shock with respect to the one generated by the laser pulse, in the emulated Schlieren image reported in Figure 9(f) ($t = 150\,\mu$s), the new shock wave is not clearly visible. However, the



DOI: 10.1002/fld

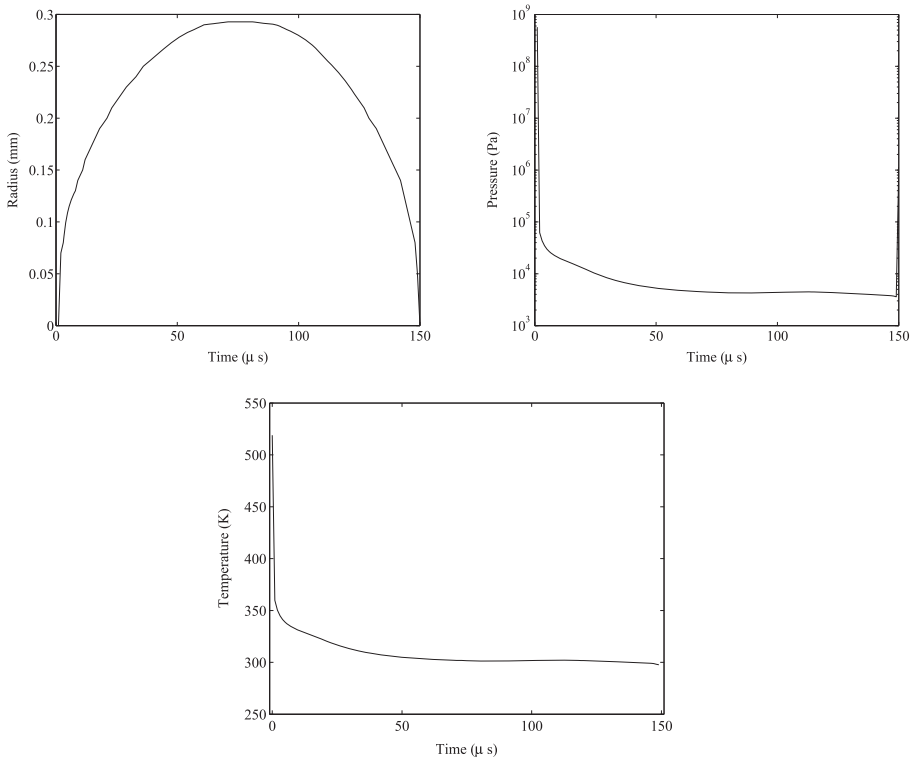


Figure 10. Laser-induced cavitation bubble: growth and collapse of the vapor bubble. On the left panel, the bubble radius is plotted versus time, while on the right panel, the pressure at the center of the bubble is plotted.

presence of this shock wave is highlighted in the right side of Figure 9(f) where the positive radial velocity indicates that a shock wave is propagating toward the boundary of the domain.

The bubble radius and the pressure at the center of the bubble are also reported in Figure 10. Comparing the oscillation time and the maximum radius of the bubble with the data reported in [19], we notice that these results are not in agreement with real observation. This can be related to the fact that we are considering a 2D bubble, instead of a 3D one as in the laboratory experiment. Furthermore, as in the numerical simulation presented in [42], there is no rebound of the bubble after the collapse. In real experiments, this behavior is not observed, and it is thought to be due to the presence of a percentage of noncondensable gas inside the bubble beside the water vapor [42, 43]. However, from the data collected, the model is able to properly reproduce the dynamics of the problem, that is, the bubble and the shock generation, the bubble expansion and collapse, and the consequent generation of the new shock.

## 7. CONCLUSIONS

In this paper, the thermodynamically compatible system of conservation laws proposed in [14, 15] for two-phase flow with a single temperature and different pressures and velocities is extended, introducing phase transition. The fluid thermodynamics has been restricted to the 'stiffened gas' equations of state because it was sufficiently accurate for the applications.

The governing equations form a hyperbolic system and are written in conservative form, allowing the use of central finite-volume schemes. The modification of Kurganov, Noelle, and Petrova numerical fluxes [15], in the framework of the second-order MUSCL-Hancock method, was employed to develop a new multidimensional solver within the parallel open-source CFD software package OpenFOAM.



DOI: 10.1002/fld

Three cavitation problems with different relaxation timescales have been studied. A comparison of the results with previous works showed good agreement with the results obtained with different numerical schemes and different governing equations.

## APPENDIX A

### *A.1. Eigenvalue evaluation*

In Section 4, we have shown that two characteristic speeds equal the mixture velocity, and, for the reduced matrix $A$ defining the remaining four characteristic speeds, we have written explicitly the characteristic polynomial coefficients, defined as functions of known quantities and of the derivatives $\partial \tilde{p}_i/\partial \rho_j$ and $\partial \tilde{T}/\partial \rho_j$. A possibility to evaluate the roots of the polynomial is to evaluate these terms solving the system of equation (48) for $\tilde{s}_1$ and $\tilde{s}_2$, in order to write explicitly the expressions for $\tilde{p}_i(\alpha_1, \rho_1, \rho_2, S)$ and $\tilde{T}(\alpha_1, \rho_1, \rho_2, S)$, but this approach can be expensive from a numerical point of view.

We show here that it is possible to write the two derivatives only in terms of the original equation of state (1), that is, without the need of evaluating explicitly the terms $\tilde{s}_1$ and $\tilde{s}_2$.

Using the definition of $\tilde{T}$, we can write

$$\frac{\partial \tilde{T}}{\partial \rho_j} = \frac{\partial}{\partial \rho_j} T_j(\rho_j, \tilde{s}_j) = \frac{\partial T_j}{\partial \rho_j} + \frac{\partial T_j}{\partial s_j}\frac{\partial \tilde{s}_j}{\partial \rho_j}. \tag{A.1}$$

Now, from the system of equation (48), we define the function $G$ as

$$G(\alpha_1, \rho_1, \rho_2, \tilde{s}_2, S) = c_1 T_{1,\rho_1}^{-1}(T_2(\rho_2, \tilde{s}_2)) + c_2 \tilde{s}_2 - S = 0, \tag{A.2}$$

where $T_{1,\rho_1}^{-1}(\cdot)$ is the inverse function of $T_1(\rho_1, \cdot)$ with respect to the entropy $s_1$ (i.e., $s_1 = T_{1,\rho_1}^{-1}(T)$), and using the implicit function theorem, we can write

$$\begin{aligned}
\frac{\partial \tilde{s}_2}{\partial \rho_2} &= -\frac{G_{\rho_2}}{G_{\tilde{s}_2}} = -\frac{\frac{\partial c_1}{\partial \rho_2} T_{1,\rho_1}^{-1}(T_2(\rho_2,\tilde{s}_2)) + c_1 \frac{\partial T_{1,\rho_1}^{-1}}{\partial T}\frac{\partial T_2}{\partial \rho_2} + \frac{\partial c_2}{\partial \rho_2} s_2}{c_1 \frac{\partial T_1^{-1}}{\partial T}\frac{\partial T_2}{\partial s_2} + c_2} \\
&= -\frac{\frac{\partial c_1}{\partial \rho_2} s_1 + c_1 \frac{\partial T_2}{\partial \rho_2}/\frac{\partial T_1}{\partial s_1} + \frac{\partial c_2}{\partial \rho_2} s_2}{c_1 \frac{\partial T_2}{\partial s_2}/\frac{\partial T_1}{\partial s_1} + c_2} = -\frac{\frac{\partial c_1}{\partial \rho_2}(s_1 - s_2) + c_1 \frac{\partial T_2}{\partial \rho_2}/\frac{\partial T_1}{\partial s_1}}{c_1 \frac{\partial T_2}{\partial s_2}/\frac{\partial T_1}{\partial s_1} + c_2} \\
&= -\frac{\frac{\partial c_1}{\partial \rho_2}(s_1 - s_2)\frac{\partial T_1}{\partial s_1} + c_1 \frac{\partial T_2}{\partial \rho_2}}{c_1 \frac{\partial T_2}{\partial s_2} + c_2 \frac{\partial T_1}{\partial s_1}}.
\end{aligned} \tag{A.3}$$

In the same way, from the system of equation (48), we define the function $H$ as

$$H(\alpha_1, \rho_1, \rho_2, \tilde{s}_1, S) = c_2 T_{2,\rho_2}^{-1}(T_1(\rho_1, \tilde{s}_1)) + c_2 \tilde{s}_2 - S = 0, \tag{A.4}$$

and we obtain

$$\begin{aligned}
\frac{\partial \tilde{s}_1}{\partial \rho_1} &= -\frac{H_{\rho_1}}{H_{\tilde{s}_1}} = -\frac{\frac{\partial c_2}{\partial \rho_1} T_{2,\rho_2}^{-1}(T_1(\rho_1,\tilde{s}_1)) + c_2 \frac{\partial T_{2,\rho_2}^{-1}}{\partial T}\frac{\partial T_1}{\partial \rho_1} + \frac{\partial c_1}{\partial \rho_1} s_1}{c_2 \frac{\partial T_2^{-1}}{\partial T}\frac{\partial T_1}{\partial s_1} + c_1} \\
&= -\frac{\frac{\partial c_2}{\partial \rho_1} s_2 + c_2 \frac{\partial T_1}{\partial \rho_2}/\frac{\partial T_2}{\partial s_2} + \frac{\partial c_1}{\partial \rho_1} s_1}{c_2 \frac{\partial T_1}{\partial s_1}/\frac{\partial T_2}{\partial s_2} + c_1} = -\frac{\frac{\partial c_2}{\partial \rho_1}(s_1 - s_2) + c_2 \frac{\partial T_1}{\partial \rho_1}/\frac{\partial T_2}{\partial s_2}}{c_2 \frac{\partial T_1}{\partial s_1}/\frac{\partial T_2}{\partial s_2} + c_1} \\
&= -\frac{\frac{\partial c_2}{\partial \rho_1}(s_1 - s_2)\frac{\partial T_2}{\partial s_2} + c_2 \frac{\partial T_1}{\partial \rho_1}}{c_2 \frac{\partial T_1}{\partial s_1} + c_1 \frac{\partial T_2}{\partial s_2}}.
\end{aligned} \tag{A.5}$$



DOI: 10.1002/fld

Now, expanding the derivatives of $\tilde{p}_i$, we can write

$$\begin{aligned}\frac{\partial \tilde{p}_i}{\partial \rho_j} &= \tfrac{\partial}{\partial \rho_j} p_i(\rho_i, \tilde{s}_i) = \delta_{ij} \tfrac{\partial p_i}{\partial \rho_j} + \tfrac{\partial p_i}{\partial s_i} \tfrac{\partial \tilde{s}_i}{\partial \rho_j} \\ &= \delta_{ij} C_j^2 + \left[ \tfrac{\partial}{\partial s_i} \left( \rho_i^2 \tfrac{\partial e_i(\rho_i, s_i)}{\partial \rho_i} \right) \right] \tfrac{\partial \tilde{s}_i}{\partial \rho_j} \\ &= \delta_{ij} C_j^2 + \rho_i^2 \tfrac{\partial T_i}{\partial \rho_i} \tfrac{\partial \tilde{s}_i}{\partial \rho_j},\end{aligned} \tag{A.6}$$

where $C_i$ is the isentropic sound speed of the $i$th phase defined as

$$C_i = \sqrt{\frac{\partial p_i(\rho_i, s_i)}{\partial \rho_i}}. \tag{A.7}$$

We observe that, to evaluate the expressions we have found for the derivatives $\partial \tilde{p}_i / \partial \rho_j$ and $\partial \tilde{T} / \partial \rho_j$, only the knowledge of the sound speeds $C_i$ and of the partial derivatives of the temperatures is requested, both defined in terms of the original equations of state ((1) and (2)). Furthermore, with $T_i = T_i(\rho_i, s_i)$, we have, independently from the particular choice of the equations of state,

$$\frac{\partial T_i}{\partial s_i} = \frac{T_i}{c_{v,i}}, \qquad \frac{\partial T_i}{\partial \rho_i} = \frac{T_i \Gamma_i}{\rho_i}, \tag{A.8}$$

where $c_{V,i}$ is the specific heat capacity at a constant volume of the $i$th phase and $\Gamma_i$ is the Grüneisen coefficient, defined in [31] as a function of the thermal expansion coefficient and the isothermal compressibility.

When all the coefficients of the characteristic polynomial of $A$ are known, it is easy to evaluate numerically its roots. First of all, because the system of equations (1–6) is hyperbolic, the characteristic polynomial has four real roots $\lambda_1 \leqslant \lambda_2 \leqslant \lambda_3 \leqslant \lambda_4$. Now, with the coefficient $a_4 > 0$, we have

$$\tilde{\pi}(\lambda) > 0, \quad \frac{\partial^2 \tilde{\pi}}{\partial \lambda^2}(\lambda) > 0 \qquad for \quad \lambda < \lambda_1 \quad or \quad \lambda > \lambda_4. \tag{A.9}$$

The positivity of both the polynomial and its second derivative ensures that the iterative Newton method

$$x_{n+1} = x_n - \frac{\tilde{\pi}(x_n)}{\tilde{\pi}'(x_n)},$$

with a starting point $x_0 < \lambda_1$, converges to the smallest eigenvalue $\lambda_1$, and that with a starting point $x_0 > \lambda_4$ converges to the largest eigenvalue $\lambda_4$. Finally, the initial guess $x_0$ can be easily determined using the Gershgorin circle theorem, or with a lower and upper estimates of the solutions of the characteristic polynomial.

## APPENDIX B

### *B.1. Solver implementation*

In this section, we discuss the implementation of the numerical scheme reported in this work using the OpenFOAM framework. OpenFOAM (Field Operation and Manipulation) is a free-source CFD package written in C++ that uses classes and templates to manipulate and operate scalar, vectorial, and tensorial fields [44]. OpenFOAM is programmed using an *object-oriented programming*, in which the programmer creates classes to represent conceptual objects in the code, classes that



DOI: 10.1002/fld

contain the data that make up the object. One of the strengths of OpenFOAM is that new solvers inherit from the OpenFOAM framework some very useful features like the use of unstructured mesh and parallelization. Furthermore, it is possible to use some built-in functions to calculate differential operators, like divergence, gradient, Laplacian, and curl. OpenFOAM offers the possibility of choosing several discretizations for these differential operators.

We report here the key steps of our solver to calculate the solution. Given a numerical solution $\mathbf{Q}^t$ at the time $t$, the solution at the new time step is computed as follows:

1. Computation of the time step $\Delta t$
2. Calculation of the primitive variables $\mathbf{U}^t$ from the conservative variables $\mathbf{Q}^t$
3. Linear reconstruction of $\mathbf{U}^t$ at the cell interfaces
   Example:

```
fvc::interpolate(p1, pos, "reconstruct(p1)")
fvc::interpolate(p1, neg, "reconstruct(p1)")
```

4. Calculation of the reconstructed conservative variables $\mathbf{Q}^{t,L}$ and $\mathbf{Q}^{t,R}$ at the cell interfaces from the primitive variables $\mathbf{U}^{t,L}$ and $\mathbf{U}^{t,R}$
5. Computation of the predictor step at the cell interfaces
6. Application of the interface relaxation
7. Calculation of the local speeds at the cell interfaces
8. Computation of the numerical fluxes
9. Computation of the solution $(\mathbf{Q}^{t+\Delta t})^*$ of the hyperbolic part of PDEs.
   Example:

```
solve( fvm::ddt(rho) + fvc::div(flux_rho) );
```

10. Computation of the solution $\mathbf{Q}^{t+\Delta t}$ integrating the source terms
11. Correction of the solution at the boundaries.

In this way, starting from $t = 0$, we can compute the solution at time $t = \Delta t$, and iterating the procedure, we can obtain the solution at the time desired.

ACKNOWLEDGEMENTS

The first author's research leading to these results has received funding from the European Research Council under the European Union's Seventh Framework Programme (FP/2007-2013)/ERC Grant Agreement no. 279802. The second author was supported by the Marie Curie Actions of the European Commission in the frame of the MAMMA project (FP7-PEOPLE-2009-IOF-251833). The third author acknowledges the financial support of the Russian Foundation for Basic Research (project 13-05-12051) and the Siberian Branch of the Russian Academy of Sciences (Integration Project No. 127). We are also grateful to two anonymous reviewers and the editor for their careful review and useful and constructive comments.

REFERENCES

1. Ishii M. *Thermo-fluid Dynamic Theory of Two-phase Flow*. Collection de la Direction des études et recherches d'Électricité de France: Eyrolles, 1975.
2. Baer M, Nunziato J. A two-phase mixture theory for the deflagration-to-detonation transition (ddt) in reactive granular materials. *International Journal of Multiphase Flow* 1986; **12**(6):861–889. DOI: 10.1016/0301-9322(86)90033-9.
3. Embid P, Baer M. Mathematical analysis of a two-phase continuum mixture theory. *Continuum Mechanics and Thermodynamics* 1992; **4**:279–312. DOI: 10.1007/BF01129333.
4. Saurel R, Abgrall R. A multiphase Godunov method for compressible multifluid and multiphase flows. *Journal of Computational Physics* 1999; **150**(2):425–467. DOI: 10.1006/jcph.1999.6187.
5. Abgrall R, Saurel R. Discrete equations for physical and numerical compressible multiphase mixtures. *Journal of Computational Physics* 2003; **186**(2):361–396.
6. Guillard H, Duval F. A Darcy law for the drift velocity in a two-phase flow model. *Journal of Computational Physics* 2007; **224**(1):288–313. DOI: 10.1016/j.jcp.2007.02.025.

7. Romenski E, Toro E. Compressible two-phase flows: Two-pressure models and numerical methods. *Computational Fluid Dynamics Journal* 2004; **13**(3):403–416.
8. Romenski E, Resnyansky A, Toro E. Conservative hyperbolic formulation for compressible two-phase flow with different phase pressures and temperatures. *Quarterly of Applied Mathematics* 2007; **65**:259–279.
9. Murrone A, Guillard H. A five equation reduced model for compressible two phase flow problems. *Journal of Computational Physics* 2005; **202**(2):664–698. DOI: 10.1016/j.jcp.2004.07.019.
10. Kreeft J, Koren B. A new formulation of Kapila's five-equation model for compressible two-fluid flow, and its numerical treatment. *Journal of Computational Physics* 2010; **229**(18):6220–6242.
11. Le Métayer O, Massoni J, Saurel R. Modelling evaporation fronts with reactive Riemann solvers. *Journal of Computational Physics* 2005; **205**(2):567–610. DOI: 10.1016/j.jcp.2004.11.021.
12. Zein A, Hantke M, Warnecke G. Modeling phase transition for compressible two-phase flows applied to metastable liquids. *Journal of Computational Physics* 2010; **229**(8):2964–2998. DOI: 10.1016/j.jcp.2009.12.026.
13. Resnyansky A, Bourne N, Millett J, Brown E. Constitutive modeling of shock response of polytetrafluoroethylene. *Journal of Applied Physics* 2011; **110**:033530–15.
14. Romenski E, Drikakis D, Toro E. Conservative models and numerical methods for compressible two-phase flow. *Journal of Scientific Computing* 2010; **42**(1):68–95.
15. La Spina G, de' Michieli Vitturi M. High-resolution finite volume central schemes for a compressible two-phase model. *SIAM Journal on Scientific Computing* 2012; **34**(6):B861—B880. DOI: 10.1137/12087089X.
16. Kapila A, Menikoff R, Bdzil J, Son S, Stewart D. Two-phase modeling of deflagration-to-detonation transition in granular materials: reduced equations. *Physics of Fluids* 2001; **13**:3002.
17. Pelanti M, Shyue KM. A mixture-energy-consistent six-equation two-phase numerical model for fluids with interfaces, cavitation and evaporation waves. *Journal of Computational Physics* 2013; **259**(0):331–357.
18. Saurel R, Petitpas F, Berry RA. Simple and efficient relaxation methods for interfaces separating compressible fluids, cavitating flows and shocks in multiphase mixtures. *Journal of Computational Physics* 2009; **228**(5):1678–1712.
19. Petkovsek R, Gregorcic P. A laser probe measurement of cavitation bubble dynamics improved by shock wave detection and compared to shadow photography. *Journal of Applied Physics* 2007; **102**(4):044909-09.
20. Toro E. *Riemann Solvers and Numerical Methods for Fluid Dynamics: A Practical Introduction*. Springer-Verlag: Berlin, Heidelberg, 2009.
21. Nessyahu H, Tadmor E. Non-oscillatory central differencing for hyperbolic conservation laws. *Journal of Computational Physics* 1990; **87**(2):408–463. DOI: 10.1016/0021-9991(90)90260-8.
22. Kurganov A, Tadmor E. New high-resolution central schemes for nonlinear conservation laws and convection-diffusion equations. *Journal of Computational Physics* 2000; **160**(1):241–282.
23. Godunov SK, Romensky E. Thermodynamics, conservation laws and symmetric forms of differential equations in mechanics of continuous media. *Computational Fluid Dynamics Review* 1995; **95**:19–31.
24. Romensky EI. Hyperbolic systems of thermodynamically compatible conservation laws in continuum mechanics. *Mathematical and Computer Modelling* 1998; **28**(10):115–130. DOI: 10.1016/S0895-7177(98)00159-9.
25. Romensky E. Thermodynamics and hyperbolic systems of balance laws in continuum mechanics. In *Godunov Methods*. Springer: US, 2001; 745–761. DOI: 10.1007/978-1-4615-0663-8_75.
26. Godunov S, Romenskii E. *Elements of Continuum Mechanics and Conservation Laws*. Springer: US, 2003.
27. Friedrichs KO. Symmetric hyperbolic linear differential equations. *Communications on Pure and Applied Mathematics* 1954; **7**(2):345–392.
28. Dafermos C. *Hyperbolic Conservation Laws in Continuum Physics* (3rd edn). Springer-Verlag: Berlin, 2009.
29. Glimm J, Saltz D, Sharp D. Two-phase modelling of a fluid mixing layer. *Journal of Fluid Mechanics* 1999; **378**: 119–143.
30. Saurel R, Gavrilyuk S, Renaud F. A multiphase model with internal degrees of freedom: application to shock-bubble interaction. *Journal of Fluid Mechanics* 2003; **495**(1):283–321.
31. Menikoff R, Plohr BJ. The Riemann problem for fluid flow of real materials. *Reviews of Modern Physics* 1989; **61**:75–130. DOI: 10.1103/RevModPhys.61.75.
32. Le Métayer O, Massoni J, Saurel R. Élaboration des lois d'état d'un liquide et de sa vapeur pour les modèles d'écoulements diphasiques. *International Journal of Thermal Sciences* 2004; **43**(3):265–276. DOI: 10.1016/j.ijthermalsci.2003.09.002.
33. Sweby PK. High resolution schemes using flux limiters for hyperbolic conservation laws. *SIAM journal on numerical analysis* 1984; **21**(5):995–1011.
34. Kurganov A, Noelle S, Petrova G. Semidiscrete central-upwind schemes for hyperbolic conservation laws and Hamilton–Jacobi equations. *SIAM Journal on Scientific Computing* 2001; **23**(3):707–740. DOI: 10.1137/S1064827500373413.
35. Goncalvès E. Numerical study of expansion tube problems: toward the simulation of cavitation. *Computers & Fluids* 2013; **72**:1–19.
36. Causon D, Mingham C. Finite volume simulation of unsteady shock-cavitation in compressible water. *International Journal for Numerical Methods in Fluids* 2013; **72**(6):632–649.
37. Saurel R, Le Métayer O. A multiphase model for compressible flows with interfaces, shocks, detonation waves and cavitation. *Journal of Fluid Mechanics* 2001; **431**:239–271.
38. Vogel A, Schweiger P, Frieser A, Asiyo MN, Birngruber R. Intraocular Nd:YAG laser surgery: laser–tissue interaction, damage range, and reduction of collateral effects. *IEEE Journal of Quantum Electronics* 1990; **26**(12):2240–2260.

39. Vogel A, Busch S, Parlitz U. Shock wave emission and cavitation bubble generation by picosecond and nanosecond optical breakdown in water. *The Journal of the Acoustical Society of America* 1996; **100**:148–165.
40. Brujan EA, Nahen K, Schmidt P, Vogel A. Dynamics of laser-induced cavitation bubbles near an elastic boundary. *Journal of Fluid Mechanics* 2001; **433**(1):251–281.
41. Brujan EA, Vogel A. Stress wave emission and cavitation bubble dynamics by nanosecond optical breakdown in a tissue phantom. *Journal of Fluid Mechanics* 2006; **558**(1):281–308.
42. Zein A, Hantke M, Warnecke G. On the modeling and simulation of a laser-induced cavitation bubble. *International Journal for Numerical Methods in Fluids* 2013; **73**(2):172–203. DOI: 10.1002/fld.3796.
43. Dreyer W, Duderstadt F, Hantke M, Warnecke G. Bubbles in liquids with phase transition. *Continuum Mechanics and Thermodynamics* 2012; **24**(4-6):461–483.
44. Weller HG. A tensorial approach to computational continuum mechanics using object-oriented techniques. *Computers in Physics* 1998; **12**:620–631. DOI: 10.1063/1.168744.